

Vacuum birefringence in strong magnetic fields:
(II) Complex refractive index from the lowest Landau level

Koichi Hattori*

*Institute of Physics and Applied Physics,
Yonsei University, Seoul 120-749, Korea*

Kazunori Itakura†

*Theory Center, IPNS, High energy accelerator research organization (KEK),
1-1 Oho, Tsukuba, Ibaraki 305-0801, Japan and
Department of Particle and Nuclear Studies,
Graduate University for Advanced Studies (SOKENDAI),
1-1 Oho, Tsukuba, Ibaraki 305-0801, Japan*

(Dated: November 10, 2018)

Abstract

We compute the refractive indices of a photon propagating in strong magnetic fields on the basis of the analytic representation of the vacuum polarization tensor obtained in our previous paper. When the external magnetic field is strong enough for the fermion one-loop diagram of the polarization tensor to be approximated by the lowest Landau level, the propagating mode in parallel to the magnetic field is subject to modification: The refractive index deviates from unity and can be very large, and when the photon energy is large enough, the refractive index acquires an imaginary part indicating decay of a photon into a fermion-antifermion pair. We study dependences of the refractive index on the propagating angle and the magnetic-field strength. It is also emphasized that a self-consistent treatment of the equation which defines the refractive index is indispensable for accurate description of the refractive index. This self-consistent treatment physically corresponds to consistently including the effects of back reactions of the distorted Dirac sea in response to the incident photon.

* khattori@yonsei.ac.kr

† kazunori.itakura@kek.jp

I. INTRODUCTION

In our recent paper which we call “paper I” [1], we analytically computed the vacuum polarization tensor of a propagating photon in a strong magnetic field at the one-loop level of a ‘dressed’ fermion, which is diagrammatically shown in Fig. 1. While the interaction of the fermion with the propagating photon (wavy lines in Fig. 1) is considered at the lowest order with respect to the coupling constant, the resultant diagram contains all-order tree-level interactions with the external field (dashed lines) through the use of the dressed fermion (a double line). Such diagrams are enhanced when the external magnetic field is strong enough, because each insertion of the external field B yields an enhancement factor $eB/m^2 = B/B_c$ where m is a mass of the fermion and $B_c \equiv m^2/e$ is the corresponding critical magnetic field. The vacuum polarization tensor, or equivalently, the self-energy of a photon is a fundamental quantity that carries information on the change of properties of a propagating photon in response to the external field.

Having obtained the analytic representation of the polarization tensor, we can now investigate *vacuum birefringence* and *decay of a photon into a fermion-antifermion pair*, both of which are characteristic phenomena of “nonlinear QED effects” and should become visible in external fields stronger than the critical magnetic field B_c . In the presence of external magnetic fields, the vacuum polarization tensor allows for additional terms which are absent in the ordinary vacuum (see Eq. (5)). These additional terms depend on polarizations of the photon, and consequently lead to birefringence phenomena. Furthermore, the polarization tensor obtained in paper I [1] is expressed as infinite summation over all the possible pairs of Landau levels corresponding to those of a fermion and of an antifermion in the magnetic field, and show quite nontrivial behavior when the photon momentum is around the thresholds of the decay determined by the Landau levels. In particular, the vacuum polarization tensor

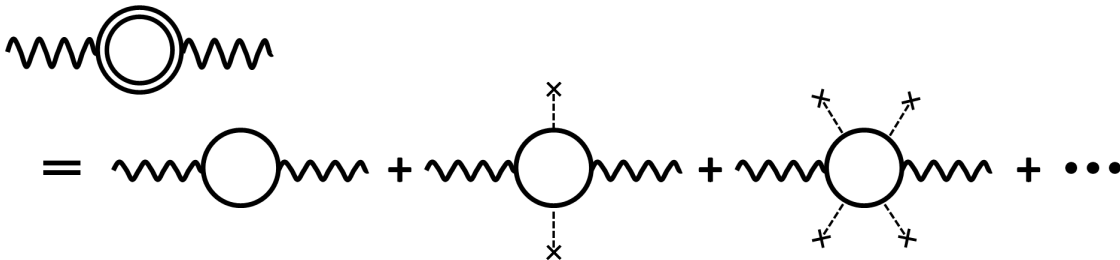


FIG. 1. Vacuum polarization in a magnetic field.

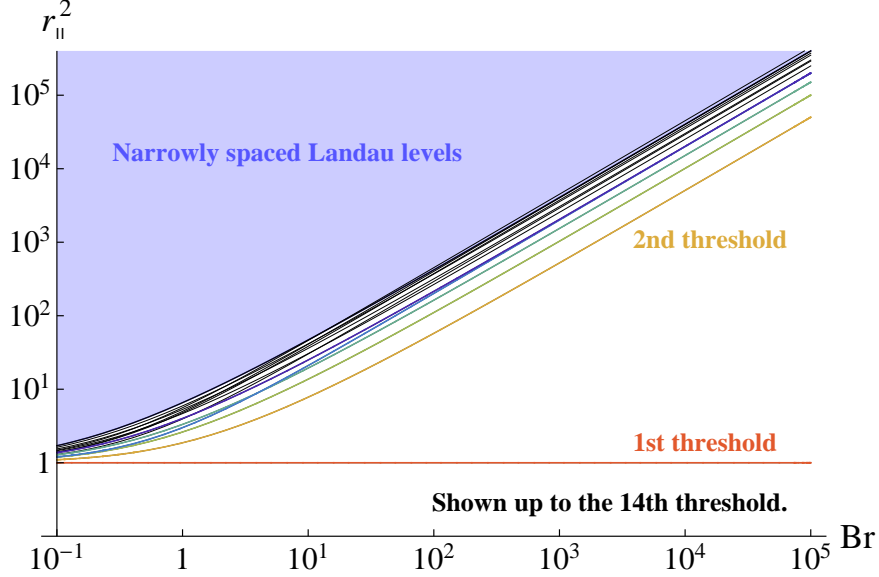


FIG. 2. Threshold structure of a photon momentum $r_{\parallel} = q_{\parallel}^2/(4m^2)$ as a function of $B_r = B/B_c = eB/m^2$. Curves are positions of thresholds $q_{\parallel}^2 = \{\sqrt{m^2 + 2\ell eB} + \sqrt{m^2 + 2(\ell + n)eB}\}^2$ with $\ell, n \in \mathbb{Z}$, determined by the Landau levels with vanishing longitudinal momenta. The shaded region is densely filled with the threshold lines. The horizontal line at $r_{\parallel}^2 = 1$ corresponds to the lowest threshold ($n = \ell = 0$).

has an imaginary part when the photon momentum is larger than the lowest threshold which indicates the decay of a photon into a pair of a fermion and an antifermion, both of which are in the lowest Landau levels with vanishing momenta along the direction of the magnetic field. Moreover, each term of the infinite summation of the polarization tensor corresponds to a pair of Landau level indices, and thus has a unique threshold determined by the Landau levels. In all the terms, an imaginary part appears when the photon momentum exceeds the threshold specific to individual terms.

In the present paper, we compute *refractive indices* and *dielectric constants* by using the analytic expression for the vacuum polarization tensor. We investigate very carefully their behavior around the thresholds, and how the imaginary part appears when the photon momentum exceeds the first threshold given by the lowest Landau levels (LLs). In fact, since all the thresholds have similar structures as that of the first threshold in the vacuum polarization tensor, we focus in the present paper on the first threshold. In other words, we consider the results in the LL approximation. This physically corresponds to working in the

strong limit of the external magnetic field because the first threshold is independent of the magnitude of the magnetic field and thus gets isolated more distantly from the higher thresholds as the magnetic field becomes stronger. This is shown in Fig. 2. Thus, our calculation in the present paper is valid below the second lowest threshold $q_{\parallel}^2 < (m + \sqrt{m^2 + 2eB})^2$.

The refractive indices n and the dielectric constants ϵ are defined through the dispersion relations for the propagating photons $\epsilon = n^2 = |\mathbf{q}^2|/\omega^2$, which one obtains by solving the Maxwell equation with the vacuum polarization tensor included [1, 2]. Then, one finds that they are in general expressed by the scalar coefficients χ_i ($i = 0, 1, 2$) of the vacuum polarization tensor (only χ_0 remains nonzero in the vanishing field limit):

$$\epsilon_{\perp} = \frac{1 + \chi_0}{1 + \chi_0 + \chi_2 \sin^2 \theta}, \quad (1)$$

$$\epsilon_{\parallel} = \frac{1 + \chi_0 + \chi_1}{1 + \chi_0 + \chi_1 \cos^2 \theta}, \quad (2)$$

where θ is the angle between the photon momentum and the magnetic field, and the perpendicular \perp and parallel \parallel indices imply polarizations with respect to the direction of the magnetic field. However, these expressions do not immediately provide the results we want. This is because the scalar functions χ_i are in general functions of the photon momentum q^μ and thus contain the refractive indices (or the dielectric constants) through the dispersion relation. Thus, to obtain the correct values for the refractive indices (and dielectric constants), one has to treat the equations self-consistently. We will see that such a self-consistent procedure gives a large effect when the deviation of the refractive indices (or the dielectric constants) from unity is large.

As is well explained in standard textbooks on optics, refractive indices have clear physical meaning: Real part of the refraction index provides a *phase velocity* $v_{\text{phase}} = 1/n_{\text{real}}$ of a propagating photon and imaginary part is called an *extinction coefficient* $\kappa = n_{\text{imag}}$ for the photon propagation. They appear in a phase factor and a damping factor of the photon field $\Psi(t, \mathbf{x})$ (see Appendix D in Ref. [1] for detail):

$$\Psi(t, \mathbf{x}) \propto \exp\{-i\omega(t - v_{\text{phase}}^{-1} \hat{\mathbf{q}} \cdot \mathbf{x})\} \exp\{-\omega \kappa \hat{\mathbf{q}} \cdot \mathbf{x}\}, \quad (3)$$

where $\hat{\mathbf{q}}$ is a unit vector directed to the photon propagation. Thus it is natural to define *decay length* in which the intensity of the photon field $I(t, \mathbf{x}) \propto |\Psi(t, \mathbf{x})|^2$ falls off in a strong magnetic field,

$$d \equiv \frac{1}{2\omega\kappa} = \frac{1}{2\omega n_{\text{imag}}}. \quad (4)$$

When the refractive index has an imaginary part, the decay length takes a finite value, which also indicates that the photon decays within a finite lifetime. Notice that these quantities depend on the photon energy ω and the angle θ between the magnetic field and the photon propagation direction. In fact, they are phenomenologically important when we apply our results to realistic situations such as in heavy-ion collisions and high-intensity laser where strong magnetic fields are realized only in a small space-time volume. Namely, if decay length and lifetime are small enough compared to the spatial extent and time duration of strong magnetic fields, then the decay process will be dominant. Otherwise only the birefringence phenomena will be seen.

The present paper is organized as follows: in the next section, we briefly review the main results obtained in paper I. In particular, we give the explicit form of the vacuum polarization tensor in the LLL approximation which is used in the present paper. Since the perpendicular polarization of the dielectric constant is not modified ($\epsilon_{\perp} = 1$) in the LLL approximation¹, we will discuss only the parallel polarization ϵ_{\parallel} in the following sections. In Sec. III, we discuss general aspects of the dielectric constant in the LLL approximation, which is followed by detailed description in Sec. IV. There, we compare results from different methods in solving the self-consistent equation for the dielectric constant. Then, in Sec. V, we show the refractive index of the parallel component. Since the refractive index is trivially related to the dielectric constant, the results are qualitatively the same, but still, it will be useful when we apply our results to phenomenology. The last section is devoted to summary and discussions. We point out similarities between the vacuum birefringence in a strong magnetic field and the optical properties of substances. We also comment on future applications in laser physics, heavy-ion physics, and compact stars with high magnetic fields. In Appendices, we provide some supplementary information such as the dependence of dielectric constant on the propagation angle and the magnetic field strength, and a brief comment on other higher Landau levels.

¹ The other contributions from the higher Landau levels barely modify the perpendicular polarization ϵ_{\perp} in the kinematical region below the lowest threshold. This will be briefly mentioned again in associate with Fig. 4.

II. VACUUM POLARIZATION TENSOR IN STRONG MAGNETIC FIELDS

In this section, we briefly summarize the main results obtained in paper I [1]. We also provide notations necessary for the calculation in the present paper. As we mentioned in Introduction, we work in the strong field limit and thus we present here the explicit analytic expression of the vacuum polarization tensor in the LLL approximation.

A. Vacuum polarization tensor and dielectric constants

Suppose that the external magnetic field is applied along the third axis of spatial coordinates in the negative direction so that $eB^3 = |e|B > 0$ for an electron ($B^3 = -B$ is the third component of the magnetic field vector B^i , and $e = -|e|$ is negative for an electron). The photon momentum q^μ is now decomposed into longitudinal and transverse components with respect to the magnetic field, namely $q_\parallel^\mu = (q^0, 0, 0, q^3)$ and $q_\perp^\mu = (0, q^1, q^2, 0)$. Correspondingly, the metric tensor $\eta^{\mu\nu} = \text{diag}(1, -1, -1, -1)$ is also decomposed into longitudinal and transverse subspaces $\eta_\parallel^{\mu\nu} = \text{diag}(1, 0, 0, -1)$ and $\eta_\perp^{\mu\nu} = \text{diag}(0, -1, -1, 0)$.

In the absence of the full Lorentz symmetry, the vacuum polarization tensor $\Pi_{\text{ex}}^{\mu\nu}(q_\parallel, q_\perp; B_r)$ allows for two additional terms. Using the projection operators $P_i^{\mu\nu}$ satisfying $q_\mu P_i^{\mu\nu} = 0$, a gauge-invariant tensor structure is given by [2–6] (see also Ref. [1] and Refs. [7, 8] for details),

$$\Pi_{\text{ex}}^{\mu\nu}(q_\parallel, q_\perp; B_r) = -\left(\chi_0 P_0^{\mu\nu} + \chi_1 P_1^{\mu\nu} + \chi_2 P_2^{\mu\nu}\right), \quad (5)$$

$$P_0^{\mu\nu} = q^2 \eta^{\mu\nu} - q^\mu q^\nu, \quad P_1^{\mu\nu} = q_\parallel^2 \eta_\parallel^{\mu\nu} - q_\parallel^\mu q_\parallel^\nu, \quad P_2^{\mu\nu} = q_\perp^2 \eta_\perp^{\mu\nu} - q_\perp^\mu q_\perp^\nu, \quad (6)$$

where we suppressed arguments of Lorentz-scalar coefficient functions χ_i ($i = 0, 1, 2$). All the three coefficient functions depend on the magnetic field $B_r = B/B_c$ and the photon momentum, $q^\mu = q_\parallel^\mu + q_\perp^\mu$. One can show that the vacuum polarization tensor in the ordinary vacuum is appropriately reproduced in the vanishing magnetic field limit: χ_0 results in the coefficient function of the vacuum polarization tensor in the ordinary vacuum, while the other two $\chi_{1,2}$ vanish.

Plugging the general form of the polarization tensor (5) into the Maxwell equation for the propagating photon, we can solve it to obtain the dispersion relations for physical modes (see Sec. 3 and Appendices C and D in paper I [1]). As mentioned in Introduction, the

dielectric constants ϵ or the refractive indices n are defined by

$$\epsilon = n^2 = \frac{|\mathbf{q}|^2}{\omega^2}, \quad (7)$$

where the photon momentum is $q^\mu = (\omega, \mathbf{q})$. Then, one finds two different values ϵ_\perp and ϵ_\parallel for the dielectric constants as shown in Eqs. (1) and (2). There, we have taken a coordinate system in which a photon is propagating in the $y = 0$ plane so that the momentum vector q^μ is represented as $q^\mu = (\omega, |\mathbf{q}| \sin(\pi - \theta), 0, |\mathbf{q}| \cos(\pi - \theta))$ with θ being the angle between the direction of the external magnetic field and the momentum of a propagating photon.

Since two dielectric constants ϵ_\perp and ϵ_\parallel , and consequently, two refractive indices n_\perp and n_\parallel , are in general not equal to unity and different from each other, we call this phenomenon *vacuum birefringence* after a similar phenomenon in dielectric substances. Notice also that, due to the violation of the Lorentz symmetry by an external magnetic field, the dielectric constants explicitly depend on the zenith angle θ . Nevertheless, the system maintains boost invariance in the third direction, and thus photon propagations in the directions at $\theta = 0, \pi$ are special. Indeed, substituting these angles into Eqs. (1) and (2), we find that both of them become unity $\epsilon_\perp(\theta = 0, \pi) = \epsilon_\parallel(\theta = 0, \pi) = 1$ and that there is no effect from the magnetic field.

As we will discuss later and also discussed in detail in paper I [1], the scalar coefficients can become complex when the photon momentum exceeds some threshold values. In that case, the corresponding dielectric constants and refractive indices are also complex. Since the scalar coefficients χ_i are parts of the self-energy of the photon, emergence of an imaginary part indicates the decay of a photon into a fermion-antifermion pair.

B. Scalar coefficient functions in the LLL approximation

Let us outline how to obtain analytic representations for the scalar coefficient functions χ_i in the external magnetic fields. In paper I, we computed χ_i by Schwinger's proper time method which is a very useful technique for the calculations under external fields [9]. Each coefficient function was first expressed as a double integral with respect to two proper times, each of which is associated with the fermion propagator composing the fermion loop (see Fig. 1). Then, the integration was analytically performed after we made rapidly oscillating integrands tractable by expanding them with known special functions. The results

we obtained are represented as infinite summation with respect to two indices, which are afterward identified with the Landau levels. In particular, the first term in the double infinite sum corresponds to the contribution of the lowest Landau levels, which was confirmed to agree with expressions obtained by other approximate methods in the strong field limit [2, 10]. We will investigate this contribution in detail in the present work. See paper I for details of the calculation and the explicit analytic forms of all the scalar coefficient functions [1].

Here we just show the explicit form of the coefficient functions from the lowest Landau levels. Below, we use the following notations for dimensionless kinematical variables: $r_{\parallel}^2 = q_{\parallel}^2/(4m^2)$ and $r_{\perp}^2 = q_{\perp}^2/(4m^2) = -|\mathbf{q}_{\perp}|^2/(4m^2)$. We also use a shorthand notation: $\eta \equiv -2r_{\perp}^2/B_r$. By taking the first term in the sum with respect to the Landau levels (see Sec. 4.2 in paper I [1] for details), we find that the coefficient functions χ_i of the vacuum polarization tensor survive only for $i = 1$:

$$\chi_0^{\text{LLL}} = \chi_2^{\text{LLL}} = 0, \quad (8)$$

$$\chi_1^{\text{LLL}}(r_{\parallel}^2, r_{\perp}^2; B_r) = \frac{\alpha B_r}{4\pi} e^{-\eta} \times \frac{1}{r_{\parallel}^2} \{I_{0\Delta}^0(r_{\parallel}^2) - 2\}, \quad (9)$$

where $\alpha = e^2/(4\pi)$ and $I_{0\Delta}^0(r_{\parallel}^2)$ is a function responsible for the threshold behavior at the lowest Landau level. Note that the dynamics encoded in the above expression is interpreted in terms of the factorized dependence on the photon momenta, r_{\parallel}^2 and r_{\perp}^2 . A Gaussian factor, $\frac{|eB|}{2\pi} \cdot \exp(-|\mathbf{q}_{\perp}|^2/(2|eB|))$, corresponds to the wave function of an electron in the lowest Landau level representing the degeneracy factor for the angular momentum and the transverse extension, while the rest part agrees with the free photon vacuum polarization tensor in 1+1 dimensions. This structure reflects the motion of an electron in strong magnetic fields restricted in the longitudinal direction, which is termed “dimensional reduction” (see, e.g., Refs. [10, 11] and references therein).

Depending on the value of r_{\parallel}^2 , the piecewise expression of $I_{0\Delta}^0(r_{\parallel}^2)$ is given as

$$I_{0\Delta}^0(r_{\parallel}^2) = \begin{cases} \frac{1}{\sqrt{r_{\parallel}^2(r_{\parallel}^2-1)}} \ln \left| \frac{r_{\parallel}^2 - \sqrt{r_{\parallel}^2(r_{\parallel}^2-1)}}{r_{\parallel}^2 + \sqrt{r_{\parallel}^2(r_{\parallel}^2-1)}} \right| & (r_{\parallel}^2 < 0) \\ \frac{2}{\sqrt{r_{\parallel}^2(1-r_{\parallel}^2)}} \arctan \left\{ \frac{r_{\parallel}^2}{\sqrt{r_{\parallel}^2(1-r_{\parallel}^2)}} \right\} & (0 < r_{\parallel}^2 < 1) \\ \frac{1}{\sqrt{r_{\parallel}^2(r_{\parallel}^2-1)}} \left[\ln \left| \frac{r_{\parallel}^2 - \sqrt{r_{\parallel}^2(r_{\parallel}^2-1)}}{r_{\parallel}^2 + \sqrt{r_{\parallel}^2(r_{\parallel}^2-1)}} \right| + \pi i \right] & (1 < r_{\parallel}^2) \end{cases} . \quad (10)$$

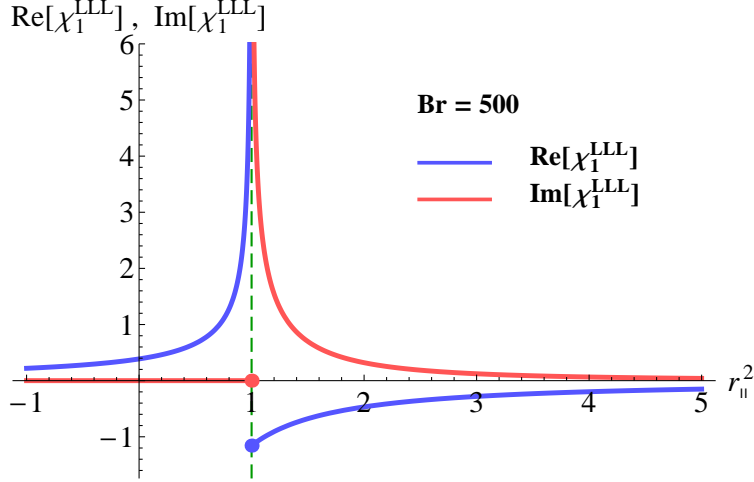


FIG. 3. The scalar function χ_1^{LLL} : blue and red lines show real and imaginary parts of χ_1^{LLL} .

Notice that this function has a singular behavior at $r_{\parallel}^2 = 1$ and that $r_{\parallel}^2 = 1$ corresponds to the lowest threshold for the decay of a photon into a fermion-antifermion pair. This is confirmed by the following observations. Firstly, the function $I_{0\Delta}^0(r_{\parallel}^2)$, and thus the scalar function χ_1^{LLL} , has an imaginary part in the region, $r_{\parallel}^2 > 1$. Next, as briefly commented in Introduction and shown in paper I [1], each term in the infinite summation of the coefficient functions is specified by two integers n and ℓ , and acquires an imaginary part as the photon momentum increases beyond the threshold value $r_{\parallel}^2 = \left\{ \sqrt{1 + 2\ell B_r} + \sqrt{1 + 2(\ell + n)B_r} \right\}^2 / 4$. This representation of the threshold suggests that ℓ and $\ell + n$ can be interpreted as the Landau levels of a fermion and an antifermion. From these, one finds that the condition $r_{\parallel}^2 = 1$ is realized by the lowest Landau levels $\ell = n = 0$, and thus emergence of an imaginary part in $r_{\parallel}^2 > 1$ implies the decay of a photon into a fermion-antifermion pair in the lowest Landau levels. Note also that $I_{0\Delta}^0(r_{\parallel}^2)$ does not depend on B_r , reflecting the fact that the location of the threshold for the lowest Landau level, $r_{\parallel}^2 = 1$, is independent of B_r . Therefore, within the LLL approximation, the coefficient function χ_1^{LLL} linearly scales as the magnetic-field strength B_r increases when $r_{\perp}^2 \ll B_r$ (see Eq. (9)), which will be also seen in Fig. 4 when the photon momentum is below the lowest threshold. Finally, it should be emphasized that $r_{\parallel}^2 = 1$ is the only one singular point of the function $I_{0\Delta}^0(r_{\parallel}^2)$. Indeed, it is continuous at $r_{\parallel}^2 = 0$ with a finite value $I_{0\Delta}^0(0) = 2$, without any singularity. In Fig. 3, we show the behavior of the scalar function χ_1^{LLL} around the threshold $r_{\parallel}^2 = 1$. The other thresholds from higher Landau levels have qualitatively the same structure as shown in Fig. 3.

III. GENERALITIES ON DIELECTRIC CONSTANT IN THE LLL APPROXIMATION

By using the analytic expression of the vacuum polarization tensor, we can compute the dielectric constants given in Eqs. (1) and (2). In this section, we discuss some general aspects of the dielectric constants and the difficulties in computing them from the coefficient functions χ_i . A complete description of the dielectric constant within the LLL approximation will be presented in the next section.

First of all, we emphasize that we have not yet specified any dispersion relation for the external photon momentum in the scalar coefficient functions χ_i . For an on-shell photon, the dispersion relations should be determined by Eqs. (1) and (2), which do contain the dielectric constants on the right-hand sides through the photon momenta, r_{\parallel}^2 and r_{\perp}^2 . According to the definition of the dielectric constant (7), those photon momenta are written as, $r_{\parallel}^2 = \tilde{\omega}^2(1 - \epsilon \cos^2 \theta)$ and $r_{\perp}^2 = -\epsilon \tilde{\omega}^2 \sin^2 \theta$, commonly for ϵ_{\perp} and ϵ_{\parallel} , where we introduced a scaled photon energy, $\tilde{\omega}^2 = \omega^2/(4m^2)$. This fact indicates that we have to solve these relations in a self-consistent way with respect to the dielectric constant appearing on the both sides. As we will find later, there is a large deviation from the massless-type dispersion relation indicating that $r_{\parallel}^2 + r_{\perp}^2 \neq 0$ and $\omega \neq |\mathbf{q}|$. We will see that a self-consistent treatment plays an important role in such a case. In particular, we will investigate very carefully how the presence of the threshold and an imaginary part in χ_i affects the results, which can be well studied in the LLL approximation.

Within the LLL approximation, only χ_1 is nonzero as shown in Eqs. (8) and (9). It immediately follows from Eq. (1) that the dielectric constant in one of the polarization modes is intact, $\epsilon_{\perp} = 1$. This is understood from following two observations. First, as shown in Appendix D in paper I [1], an electric field induced in this polarization mode oscillates perpendicularly to the external field. Second, since the discretized transverse momentum of a fermion is fixed to the lowest Landau level, motion of a vacuum pair excitation is restricted only along the external magnetic field. Because the direction of the possible dipole excitation is perpendicular to the electric field accompanying this polarization mode, this mode does not induce an electric dipole excitation. Therefore, its propagation is not modified. On the other hand, an electric field accompanying the other polarization mode has a parallel component oscillating along the external magnetic field. Thus, an electric dipole can be

induced as a response of the Dirac sea, which results in a modification of the dielectric constant ϵ_{\parallel} shown in Eq. (2).

Inserting $\chi_0 = \chi_2 = 0$ into the general expressions (1) and (2), we find the dielectric constants in the LLL approximation:

$$\epsilon_{\perp}^{\text{LLL}} = 1, \quad (11)$$

$$\epsilon_{\parallel}^{\text{LLL}}(\tilde{\omega}, \theta; B_r) = \frac{1 + \chi_1^{\text{LLL}}(r_{\parallel}^2, r_{\perp}^2; B_r)}{1 + \chi_1^{\text{LLL}}(r_{\parallel}^2, r_{\perp}^2; B_r) \times \cos^2 \theta}. \quad (12)$$

Here, we have explicitly shown the arguments of $\epsilon_{\parallel}^{\text{LLL}}$ and χ_1^{LLL} . The dielectric constant $\epsilon_{\parallel}^{\text{LLL}}$ depends on a scaled photon energy $\tilde{\omega}^2 \equiv \omega^2/(4m^2)$ and angle θ separately, because of an explicit θ -dependence on the right-hand side. It should be noticed that photon's squared momenta on the right-hand side can be rewritten in terms of the scaled energy $\tilde{\omega}$ so that they contain the dielectric constant $\epsilon_{\parallel}^{\text{LLL}}$ according to the definition (7):

$$r_{\parallel}^2 = \tilde{\omega}^2(1 - \epsilon_{\parallel}^{\text{LLL}} \cos^2 \theta), \quad (13)$$

$$r_{\perp}^2 = -\tilde{\omega}^2 \epsilon_{\parallel}^{\text{LLL}} \sin^2 \theta. \quad (14)$$

The expression of the dielectric constant (12) has to be solved with respect to ϵ_{\parallel} . We will discuss in detail that this procedure plays an important role when modification of the dielectric constant becomes sizable.

The vacuum birefringence in the LLL approximation bears an analogy to ‘uniaxial’ birefringent material, of which optical axis corresponds to a preferred orientation provided by the external magnetic field. In this analogy, the polarization mode having the dielectric constant ϵ_{\parallel} could be called “*extraordinary mode*”, while the other one having ϵ_{\perp} “*ordinary mode*”. However, this analogy holds only in the LLL approximation because the perpendicular part ϵ_{\perp} in general depends on the angle θ . Thus, if one looks at the wide range of kinematical region, the vacuum birefringence is much more complicated than the birefringence in uniaxial materials.

A. Below threshold: Accuracy check of the LLL approximation

Consider first the region below the threshold $r_{\parallel}^2 < 1$. As long as the photon momentum is in this region, one can *numerically* perform the double integration in a safe way.² Since

² Each function χ_i contains a double integral with respect to two proper-time variables τ_1 and τ_2 , and the integration over $\tau = eB(\tau_1 + \tau_2)/2$ in general suffers from strong oscillation of the integrand. However,

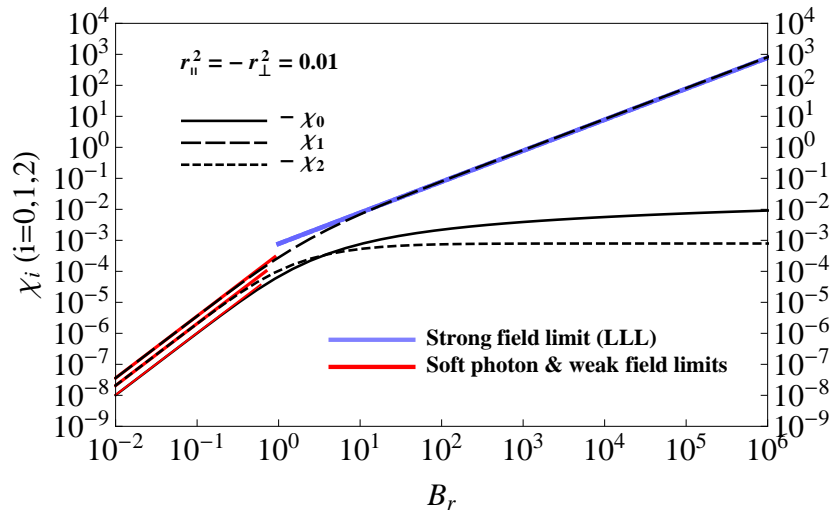


FIG. 4. B_r -dependence of the scalar functions χ_i ($i = 0, 1, 2$): three black lines show results from numerical integration [12], and red and blue lines show the weak-field [5] and strong-field (LLL) limits, respectively.

the original double integrals are directly evaluated (without being expanded with respect to special functions), the numerical results should contain all the contributions from Landau levels in our analytic expression obtained in paper I [1]. Such numerical integration was performed in Ref. [12] some years ago. Thus, we can check the validity of the LLL approximation by comparing the analytic results (9) & (10) with the numerical results.

In Fig. 4, we compare the LLL results (9) & (10) for the coefficient function χ_1^{LLL} with χ_i from the numerical integration below the threshold. The results of numerical integration (three black lines) shown in Fig. 4 were reproduced by ourselves, and agree with the previous results in Ref. [12] up to small invisible numerical errors. We also show an approximate expression for soft photon and weak-magnetic-field limit [5]. The photon momenta are taken to be small $r_{\parallel}^2 = -r_{\perp}^2 = 0.01$ below the threshold, as an illustration. In fact, this is in the ‘soft gamma-ray’ regime³ which corresponds to typical burst spectrum from the soft-gamma-ray repeaters as known as magnetars. The focus of Ref. [12] was the radiation from magnetars, which is the reason why they discussed the region below the threshold. The figure shows that the result of χ_1 from numerical integration agrees with analytic expressions in the weak and strong field limits. In particular, the LLL approximation in χ_1 works well

it can be shown that for $r_{\parallel}^2 < 1$ an integral contour in the complex τ -plane can be safely moved to the imaginary axis to obtain a well-behaved real-valued integral which allows for numerical evaluation [5, 12].
³ Electron mass is assumed here for the fermion mass “ m ” in r_{\parallel}^2 and r_{\perp}^2 .

for $B_r \gtrsim 10$, and the values of χ_0 and χ_2 are very small compared to unity, both of which confirm the use of the LLL approximation (8) – (9) in strong magnetic fields. As mentioned below Eq. (10), we find that χ_1 linearly scales as B_r increases in the strong magnetic field limit.

As long as the photon momentum is below the threshold $r_{\parallel}^2 < 1$, it is not technically difficult to obtain the dielectric constant and the refractive index. They have only real parts, and we can use the coefficient functions obtained by numerical integration. This was already performed in Ref. [12], where the results show that the refractive index in the parallel mode, n_{\parallel} , deviates from unity as the photon momentum approaches the threshold $r_{\parallel}^2 = 1$ from below. (Essentially the same result is shown in Fig. 5 for the dielectric constant in the parallel mode ϵ_{\parallel} .) Note that this method is valid for arbitrary strength of the external magnetic field, whose validity is however restricted to the kinematical region $r_{\parallel}^2 < 1$. It was also shown that deviation of n_{\parallel} from unity becomes larger as the magnetic field strength increases beyond the critical field strength $B_r = B/B_c \gtrsim 1$. On the other hand, the refractive index is barely modified in the weak field region below the critical field strength $B_r \lesssim 1$, when the photon momentum is below the threshold $r_{\parallel}^2 < 1$. We will compare the results from the numerical integration with those from the LLL approximation in later sections.

The refractive index in the perpendicular mode, n_{\perp} , was also examined for $r_{\parallel}^2 < 1$ in Ref. [12], and the result was reproduced by the present authors. The results do not show sizable deviation from unity, even when the magnetic field strength becomes larger than the critical field strength and when the photon momentum approaches the lowest threshold. Figure 4 shows that χ_0 and χ_2 are smaller than unity by two orders in magnitude, and thus they bring in only tiny modification in the dielectric constant ϵ_{\perp} in Eq. (1), and also in the refractive index n_{\perp} . These results are quantitatively consistent with the dielectric constant (11) in the LLL approximation.

B. Beyond threshold: Appearance of imaginary part

Before we present complete self-consistent treatment of the dielectric constant, we explain how the dielectric constant behaves around the threshold in a very rough estimate. First of all, let us briefly recall the behavior of χ_1^{LLL} given in Eqs. (9) and (10) around the threshold. As described below Eq. (10), the function χ_1^{LLL} has a singularity at the threshold $r_{\parallel}^2 = 1$.

When r_{\parallel}^2 goes beyond 1, it starts to have an imaginary part. The real and imaginary parts of χ_1^{LLL} diverge when the photon momentum approaches the threshold $r_{\parallel}^2 = 1$ from below and above, respectively (see Fig. 3). Whereas the emergence of an imaginary part in χ_1^{LLL} directly affects the dielectric constant $\epsilon_{\parallel}^{\text{LLL}}$ (namely, $\epsilon_{\parallel}^{\text{LLL}}$ starts to have an imaginary part above the threshold), we should notice that the dielectric constant takes a real finite value⁴ at the threshold owing to cancellation of the divergences between the numerator and denominator in Eq. (12). In fact, we find a simple expression for the value of ϵ_{\parallel} at the threshold (for $\cos \theta \neq 0$):

$$\lim_{r_{\parallel}^2 \rightarrow 1 \pm 0} \epsilon_{\parallel}(r_{\parallel}^2) = \frac{1}{\cos^2 \theta} \equiv \epsilon_{\text{lim}} \quad , \quad (15)$$

when r_{\parallel}^2 approaches the threshold from both below and above. Note that the limiting value (15) is valid even if we include contributions from other levels ($\ell \neq 0$, $n \neq 0$). This is because the divergent contribution to χ_1 at the threshold dominates any finite contribution from other levels (That is why we do not put “LLL” in the above equation). The same is true for the other higher thresholds: the limiting value of ϵ_{\parallel} at each threshold comes from the contribution in χ_i which gives divergence at that point.

Figure 5 shows a plot of the dielectric constant (12) obtained with χ_1 shown in Eqs. (9) and (10) as a function of the photon energy squared $\tilde{\omega}^2$. We have taken $\theta = \pi/4$ just for illustration (then, $\epsilon_{\text{lim}} = 2$), and a relatively large value for the magnetic field $B_r = B/B_c = 500$ so that the LLL approximation is appropriate. The dielectric constant which implicitly appears on the right-hand side of Eq. (12) is, at this moment, taken to be one. Then, inserting $\epsilon_{\parallel}^{\text{LLL}} = 1$ into r_{\parallel}^2 given by Eq. (13), one finds that the threshold condition $r_{\parallel}^2 = 1$ is now represented in the energy space as⁵ $\tilde{\omega}^2 = 1/(1 - \cos^2 \theta) = 2$ for $\theta = \pi/4$. The region $\tilde{\omega}^2 < 2$ filled with light blue color in Fig. 5 corresponds to the one below the threshold, while the region $\tilde{\omega}^2 > 2$ with pale red, beyond the threshold.

First let us see the region below the threshold. Green dots correspond to the dielectric constant ϵ_{\parallel} shown in Eq. (2) obtained on the basis of the numerical integration of χ_0 and χ_1 performed below the threshold⁶ (the same result as obtained in Ref. [12]). On the other

⁴ This is trivially true as long as $\cos^2 \theta$ is not zero, $\theta \neq \pm\pi/2$. In two particular cases at $\theta = \pm\pi/2$, the dielectric constant is given by $\epsilon_{\parallel} = 1 + \chi_1^{\text{LLL}}$ with $r_{\parallel}^2 = \tilde{\omega}^2$, which directly reflects the behavior of χ_1^{LLL} , and

is also real below the threshold. These angle-dependent behaviors will be again mentioned in Sec. V A.

⁵ Note that this equation is true only in the naive prescription where we assume $\epsilon_{\parallel}^{\text{LLL}} = 1$ in r_{\parallel}^2 .

⁶ To remove the divergence of χ_0 , we have employed a cut-off and renormalization condition described in the Appendix B in paper I [1].

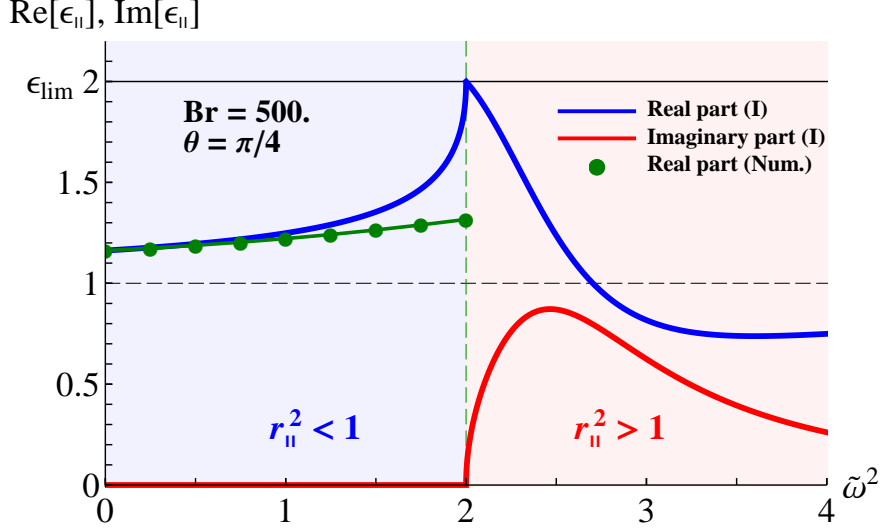


FIG. 5. Dielectric constant in the LLL approximation: blue and red lines show the real and imaginary parts of the right-hand side of Eq. (12) with $\epsilon_{\parallel}^{\text{LLL}} = 1$ in χ_1^{LLL} (called solution (I) in Sec. IV A) Filled backgrounds indicate the kinematical regimes below and above $r_{\parallel}^2 = 1$ whose boundary is given by $\tilde{\omega}^2 = 1/(1 - \cos^2 \theta)$ assuming $\epsilon_{\parallel}^{\text{LLL}} = 1$ in r_{\parallel}^2 . Green dots show the numerical computation of the real part in $r_{\parallel}^2 < 1$.

hand, a blue line corresponds to the result from the LLL approximation. As we already discussed in the previous subsection, both results grow with increasing photon energies. We will discuss the deviation between these two in the next subsection. The imaginary part shown with a red line is exactly zero in this region.

Next, look at the region beyond the threshold, $\tilde{\omega}^2 > 2$, in Fig. 5. It is clearly seen that the dielectric constant has a sizeable imaginary part. This contribution is never described by the result from numerical integration which is valid only below the threshold. We also find that the real part shows nontrivial behavior: starting from $\text{Re}[\epsilon_{\parallel}^{\text{LLL}}] = 2$ at $\tilde{\omega}^2 = 2$, it decreases, and even becomes smaller than unity. Considering the deviation between the results from the numerical integration and the LLL approximation in the region below the threshold, we expect these results (without self-consistent treatment) will not be quantitatively accurate. We will indeed see in the next section that the solution will be greatly modified in the self-consistent treatment. What is sure at this moment is the presence of the imaginary part in this region.

C. Necessity of self-consistent description

Let us come back to the results below the threshold. We have seen that there is deviation between the results from the numerical integrations (green dots) and the LLL approximation (a blue line), and that it becomes larger as the photon energy approaches the threshold. Since the results grow with increasing photon energies, one can also say that two results show a good agreement when the dielectric constant is close to unity, but deviate from each other when it becomes large. Clearly, the analytic result with a large value of $\epsilon_{\parallel} > 1$ is not consistent with the prescription assuming $\epsilon_{\parallel} = 1$ on the right-hand side of Eq. (12). On the other hand, to obtain the result from numerical integration, Eq. (2) was solved with respect to ω with its dependence on the right-hand side taken into account. Considering the facts that the result from numerical integration should be accurate in this region and that the magnetic field is strong enough for the coefficient functions to be approximated by the LLLs, we can easily conclude that the deviation of two results nearby the threshold originates from the “inconsistent” treatment of the dielectric constant in the naive prescription.

There is another evidence for the importance of the self-consistent treatment. Note that the analytic expression of the limiting behavior shown in Eq. (15) is obtained from the divergent behavior of χ_1 when the longitudinal momentum approaches the threshold, $r_{\parallel}^2 \rightarrow 1$. Inserting the limiting value ϵ_{lim} into $r_{\parallel}^2 = \tilde{\omega}^2(1 - \epsilon_{\parallel} \cos^2 \theta)$, we however notice that, as long as $\tilde{\omega}$ is finite, r_{\parallel}^2 approaches zero when the dielectric constant approaches the limiting value ϵ_{lim} ,

$$\lim_{\epsilon_{\parallel} \rightarrow \epsilon_{\text{lim}}} r_{\parallel}^2(\epsilon_{\parallel}) = 0 \quad . \quad (16)$$

Therefore, Eqs. (15) and (16) cannot be consistent with each other. This occurs when the dielectric constant is large, and must be resolved if we treat it self-consistently.

Then, what kind of physics is involved in the self-consistent description of Eq. (12)? It is helpful to recall a microscopic picture of the propagation of a photon in an ordinary medium. Variation of the dielectric constant or the refractive index is induced by the response of the medium to the incident photon. In the present case, medium is the vacuum which is filled with fermions in the Dirac sea, and the incident photon creates a polarization in it and, when its energy is large enough, even an on-shell fermion and antifermion pair which might be, alternative to the photon decay, seen as ‘photoelectric effect’ by absorption of the incident photon. These microscopic processes will generate ‘back reactions’ leading to

screening and damping of an incident photon field. Notice that these effects are embedded in the equation as modification of the external photon momenta r_{\parallel}^2 and r_{\perp}^2 through the implicit dependences on the dielectric constant (see Eqs. (13) and (14)). Therefore, what is necessary for examining these effects is, in technical terms, to solve Eq. (12) self-consistently with respect to the dielectric constant appearing on the both sides.

IV. SELF-CONSISTENT DESCRIPTION OF DIELECTRIC CONSTANT IN THE LLL APPROXIMATION

As summarized in Sec. III C, we have observed that the naive prescription in obtaining the dielectric constant may cause the deviation between the dielectric constant from the LLL approximation and the preceding result from the numerical integration as the photon energy approaches the threshold $r_{\parallel}^2 = 1$ from below, and also that there is a contradiction between the limiting value of the dielectric constant at the threshold (15) and the behavior of the squared photon momentum (16). It will turn out, as already suggested in Sec. III C, that these two problems originate from “inconsistent” treatment of Eq. (12) with respect to the dielectric constant $\epsilon_{\parallel}^{\text{LLL}}$, and that they are not present in fully self-consistent description of Eq. (12). We will see first in the region below the lowest threshold that the self-consistent treatment indeed resolves the deviation, and then will proceed to the region above the threshold where the method of numerical integration is not valid. In this section, in order to be convinced of the importance of fully self-consistent description, we increase step by step the levels of accuracy in treating Eq. (12), eventually leading to the completely self-consistent solution.

A. Three steps towards fully self-consistent description

As discussed in Sec. III C, Eq. (12) contains nontrivial effects such as screening and damping of an incident photon field, and they are correctly described in a self-consistent description. In order to entangle these effects and understand physics consequences arising from them, we solve Eq. (12) at three different levels of accuracy (I), (II) and (III) in treating the coefficient χ_1^{LLL} . We also compare the results of these three methods with the result from numerical integration (Num.) which is valid only below the threshold.

(I) “inconsistent” solution: Instead of solving Eq. (12) with respect to $\epsilon_{\parallel}^{\text{LLL}}$, we just assume $\epsilon_{\parallel}^{\text{LLL}} = 1$ in the coefficient function χ_1^{LLL} on the right-hand side. This should be a good approximation when the deviation of $\epsilon_{\parallel}^{\text{LLL}}$ from unity is small enough. The result of this treatment was already shown in Fig. 5.

(II) partially self-consistent solution: We allow for a real part of $\epsilon_{\parallel}^{\text{LLL}}$ on the right-hand side of Eq. (12). Namely, the equation for the real part $\text{Re}[\epsilon_{\parallel}^{\text{LLL}}]$ is solved self-consistently, but the imaginary part $\text{Im}[\epsilon_{\parallel}^{\text{LLL}}]$ is just given with the scalar function χ_1^{LLL} in which $\epsilon_{\parallel}^{\text{LLL}}$ is replaced by the solution of the real part. Thus, this treatment gives a partially self-consistent solution and should be a good approximation when the imaginary part is small enough. In particular, this treatment is valid below the threshold where $\epsilon_{\parallel}^{\text{LLL}}$ does not have an imaginary part.

(III) fully self-consistent solution: We treat $\epsilon_{\parallel}^{\text{LLL}}$ in χ_1^{LLL} as a complex number, and solve the real and imaginary parts of Eq. (12) fully self-consistently to find the dependence of $\epsilon_{\parallel}^{\text{LLL}}$ on a photon energy. This is the most accurate description of the dielectric constant in the LLL approximation.

(Num.) self-consistent numerical solution below the threshold: As already mentioned in the previous sections, one can directly evaluate the scalar functions χ_i ($i = 0, 1, 2$) by numerical integration as long as the photon momentum is below the threshold $r_{\parallel}^2 < 1$. One can also solve Eqs. (1) and (2) self-consistently. However, since this is possible only below the threshold, the dielectric constants are real. This treatment should be compared with (II) and (III) below the threshold.

B. Threshold condition in self-consistent description

Before we present results for the dielectric constant in the self-consistent description, let us revisit the threshold condition $r_{\parallel}^2 = 1$. We discussed that the threshold condition $r_{\parallel}^2 = 1$ gives the threshold photon energy $\tilde{\omega}_{\text{th}}^2 = 1/(1 - \cos^2 \theta)$ (see Fig. 5), if $\epsilon_{\parallel} = 1$ is assumed in r_{\parallel}^2 . In this case, the region below the threshold is simply represented by $\tilde{\omega}^2 < \tilde{\omega}_{\text{th}}^2$ as shown in Fig. 5 (where $\tilde{\omega}_{\text{th}}^2 = 2$ for $\theta = \pi/4$). However, it should be noticed first that, if we keep

the real part of ϵ_{\parallel} in r_{\parallel}^2 , the threshold photon energy is given in an ϵ_{\parallel} -dependent form as,

$$\tilde{\omega}_{\text{th}}^2 = \frac{1}{1 - \epsilon_{\parallel} \cos^2 \theta} , \quad (17)$$

and this condition is inversely solved as,

$$\epsilon_{\parallel} = \frac{1}{\cos^2 \theta} \left(1 - \frac{1}{\tilde{\omega}_{\text{th}}^2} \right) . \quad (18)$$

The above relation (18) separates the kinematical regions below and above the threshold of photon decay. Therefore, in the ϵ_{\parallel} - $\tilde{\omega}^2$ plane, the threshold line is not just a vertical line (as shown in Fig. 5), but is a curve given by Eq. (18). Inserting the limiting value ϵ_{lim} (15) into Eq. (17), we find that the photon energy approaches infinity, $\tilde{\omega} \rightarrow \infty$, as the dielectric constant approaches the limiting value. Equivalently, Eq. (18) shows that the dielectric constant does not reach the limiting value ϵ_{lim} at $r_{\parallel}^2(\epsilon_{\parallel}) = 1$, as long as the photon energy $\tilde{\omega}$ is finite. This observation implies that the dielectric constant could stay in a real value when $\tilde{\omega}$ increases from zero to infinity, and thus that the energy dependence of the dielectric constant would be significantly modified from the one in Fig. 5 obtained without any self-consistent treatment.

C. Back reactions in complex dielectric constant

Now let us finally show results from the self-consistent description. Figure 6 is a compilation of all the results of the real and imaginary parts of the dielectric constant obtained with four different treatments from (I) to (III) and (Num.). Upper and lower panels show the real and imaginary parts, respectively. We have taken the same values for B_r and θ as in Fig. 5, namely $B_r = 500$ and $\theta = \pi/4$. The threshold boundaries specified by Eq. (18) and $r_{\parallel}^2(\epsilon_{\parallel} = 1) = 1$ are indicated with green solid and dashed lines, left (right) of which is filled with light blue (pale red) and corresponds to the region below (above) the threshold. Long dashed lines (blue and red) are the ‘‘inconsistent’’ solutions from (I), short dashed lines (purple and red) are the partially self-consistent solutions from (II), and finally thick bold lines (blue and red) are the fully self-consistent solutions from (III). These are compared with green dots which are the results of numerical integration (Num.). Notice that this is the same result as shown in Fig. 5, but is now extended to larger $\tilde{\omega}^2$ because the threshold line is modified from a vertical line to a curve and the region below the threshold (filled with light blue color) extends to infinite $\tilde{\omega}^2$.

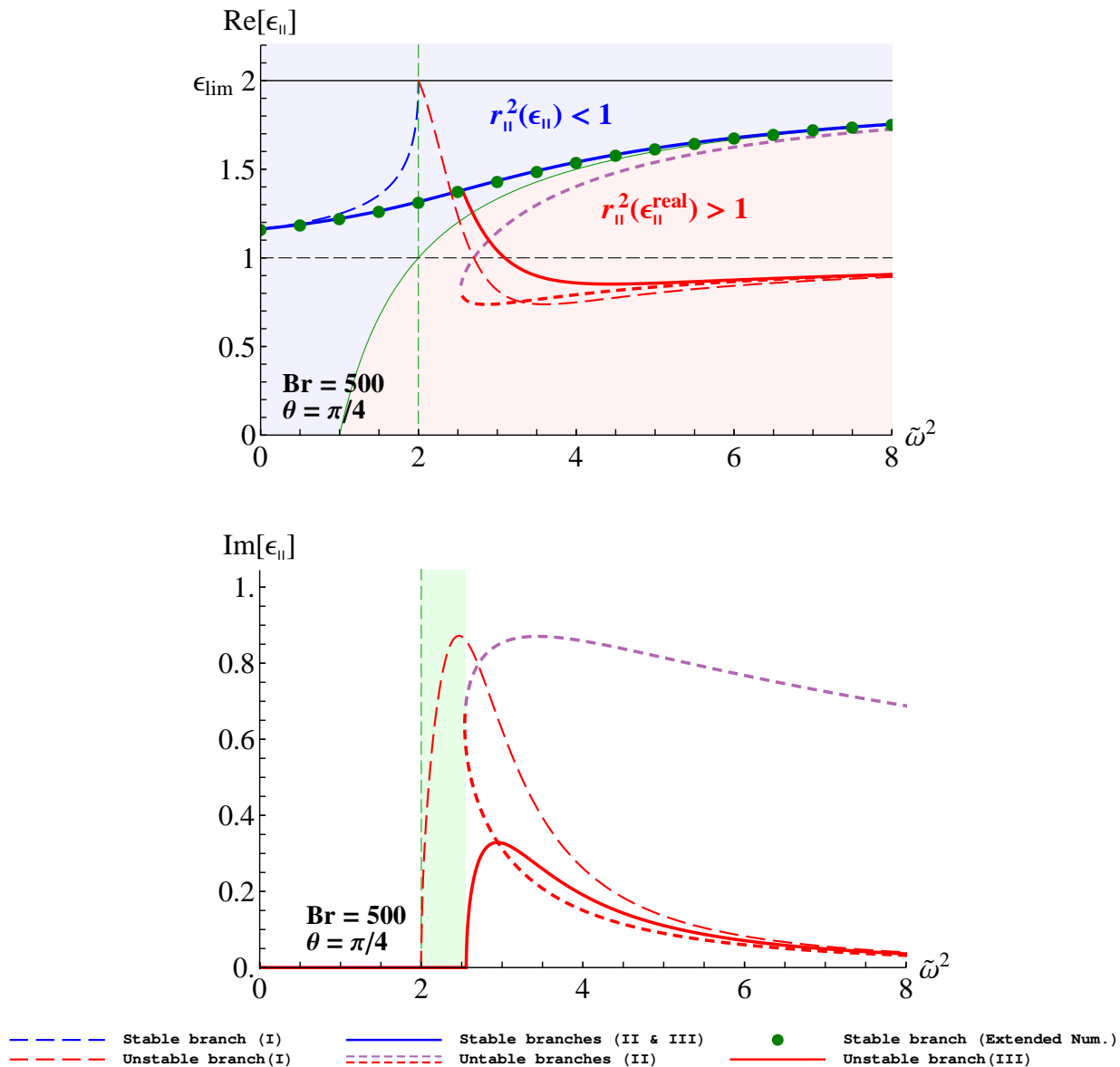


FIG. 6. Dielectric constant for $\theta = \pi/4$ and $B_r = 500$: a shift of the threshold in solution (III) from that in solution (I) is indicated with a green stripe in the lower panel.

1. Screening of incident light

Let us first consider the change from the “inconsistent” solution (I) shown as blue and red long-dashed lines, to the partially self-consistent solution (II) shown as a blue solid line and purple and red short-dashed lines. Look at the blue solid line in the upper panel, which is a common solution in treatments (II) and (III). Also, it coincides with the green dots which are from the numerical integration (Num.). Thus, as expected, the treatment (II) already

gives a final result in this region below the threshold. Since this line is not accompanied by an imaginary part at any photon energy, we call this *stable branch*. In particular, we now understand that the origin of the deviation found in Fig. 5 between the results from the LLL approximation with the naive prescription (blue long-dashed line) and the numerical integration (green dots) is the incomplete treatment of the equation (12), and that the value of the dielectric constant in the naive prescription is reduced (i.e., screened) due to back reactions. In addition to the stable branch, we found other two solutions (purple and red short-dashed lines) in the region, $r_{\parallel}^2(\epsilon_{\parallel}) > 1$. Namely, in this partially self-consistent treatment (II), we obtained the dielectric constant as a three-valued function of the photon energy $\tilde{\omega}$. The latter two branches in the region, $r_{\parallel}^2(\epsilon_{\parallel}) > 1$, smoothly connects to each other. In contrast to the solution in the region, $r_{\parallel}^2(\epsilon_{\parallel}) < 1$, these branches are accompanied by imaginary parts as shown in the lower panel, and thus we call them *unstable branches*.

As described above, the green solid line divides the kinematical regions $r_{\parallel}^2(\epsilon_{\parallel}) < 1$ and $r_{\parallel}^2(\epsilon_{\parallel}) > 1$, while the green dashed line $r_{\parallel}^2(\epsilon_{\parallel} = 1) < 1$ and $r_{\parallel}^2(\epsilon_{\parallel} = 1) > 1$. Noting a correspondence between these lines, we find that the partially self-consistent solution (II) still maintains a topological structure of (I) as correspondences between stable branches and unstable branches, respectively: the blue long-dashed (red long-dashed) line is modified to the blue solid (purple and red short-dashed) line in the solution (II). Location of the connecting point between stable and unstable branches, where the dielectric constant takes the limiting value ϵ_{lim} , has moved away from $\tilde{\omega}^2 = 1/(1 - \cos^2 \theta)$ in (I) to $\tilde{\omega}^2 = \infty$ in (II).

The lower panel in Fig. 6 shows an imaginary part of the dielectric constant associated with the unstable branches shown in the upper panel. Since the partially self-consistent solution (II) gives the double-valued unstable branch, an associated imaginary part is also a double-valued function of the photon energy. As shown with a green stripe in the background, the threshold of the photon decay shifts upward because of the modification of the real part incorporated in $r_{\parallel}^2(\epsilon_{\parallel})$.

2. Damping of incident light

Now let us see the change of solutions from (II) to (III). In partially self-consistent treatment (II), we treated the dielectric constant in χ_1^{LLL} as a real value. However, since the unstable branch has a large imaginary part (see purple short-dashed line in Fig. 6), we

should not assume that the dielectric constants in r_{\parallel}^2 and r_{\perp}^2 are real values. Physically, this indicates that we have to self-consistently take into account the damping of an incident photon due to decay into a fermion-antifermion pair in the external magnetic field when the decay rate is sizable.

We thus solve simultaneously the equations for real and imaginary parts of Eq. (12) without any assumption. This is the result of treatment (III). Maintaining both the real and imaginary parts of the dielectric constant in the photon momenta r_{\parallel}^2 and r_{\perp}^2 , we find that the structure of the branch in the kinematical region above the threshold is significantly modified. The most remarkable modification of the structure is that an unstable branch in the real part, indicated with a red solid line, directly connects to the stable branch below the threshold. According to this, the dielectric constant reduces from the three-valued function to a double-valued function of the photon energy. This edge of the unstable branch close to the connecting point is still accompanied by an imaginary part as shown in the lower panel, and thus is a state unstable to the decay. We find that a magnitude of the imaginary part is diminished in (III) compared to those of the imaginary parts obtained in the other two cases, (I) and (II). This result can be intuitively understood as follows: the magnitude of the imaginary part should be suppressed in the self-consistent treatment, since the amplitude of the incident photon damps due to the decay. Indeed, the amplitude of the photon propagation is given by the complex refractive index related to the dielectric constant as shown in Eqs. (3). In Sec. V, we will also show a complex refractive index obtained from the dielectric constant shown in this section.

D. Results in stronger magnetic field

We shall see a dielectric constant in a stronger magnetic field. Figure 7 shows the dielectric constant at much larger value of $B_r = 5000$. Each line shows the corresponding quantities indicated in the legend of Fig. 6. Compared to the results for $B_r = 500$ in Fig. 6, one finds that the modification of the real part in (I) is larger, in particular in $\tilde{\omega}^2 > 2$, with a nontrivial wavy behavior. However, as shown in red solid line of treatment (III), it is suppressed if we self-consistently incorporate a screening effect on the incident photon field caused by the induced vacuum polarization. Consequently, the real part eventually behaves similarly as in the previous case with $B_r = 500$, but its magnitude shows moderate enhancement. A

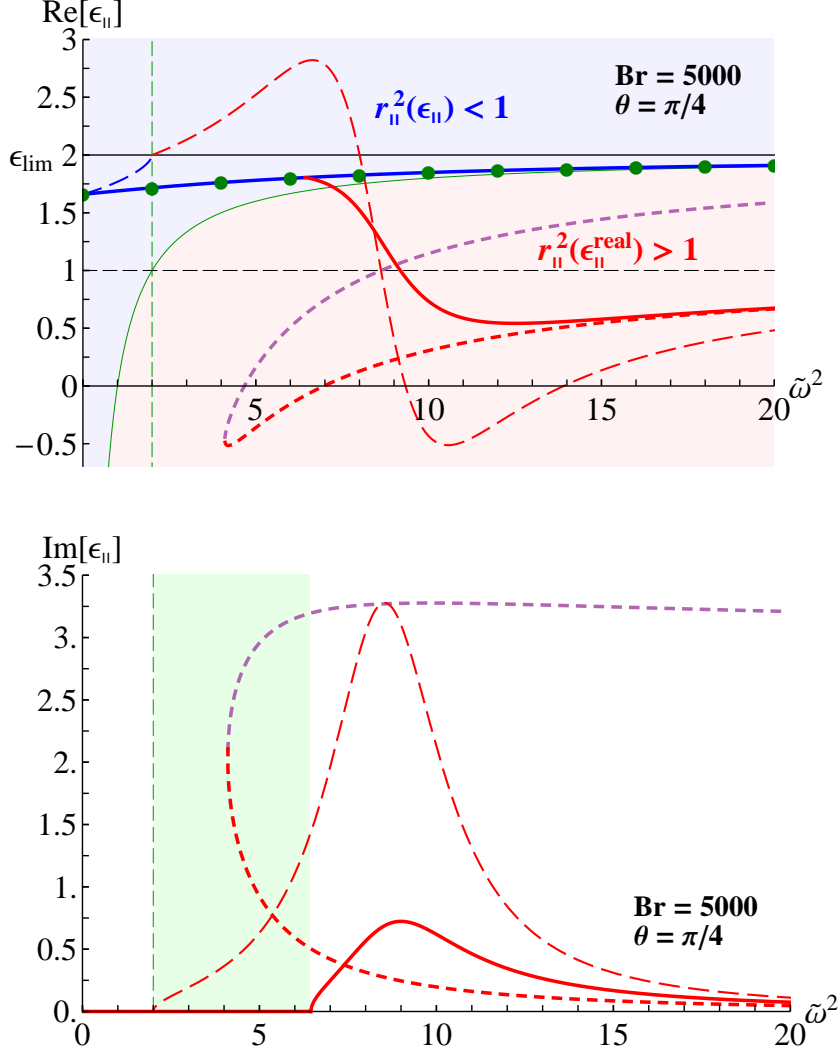


FIG. 7. Dielectric constant for $\theta = \pi/4$ and very strong magnetic field $B_r = 5000$: each line shows the corresponding quantities in the legend of Fig. 6.

significant effect of the self-consistent treatment is also found in the imaginary part. Whereas magnitudes of the imaginary parts in (I) and (II) are much larger than those in Fig. 6, they are suppressed in (III) to give moderate enhancement of the imaginary part at $B_r = 5000$, as in the real part. These results indicate that stronger distortion of the Dirac sea induces stronger effects of the competing back reactions. As for the energy dependence, the stable branch extends up to infinite photon energy as in Fig. 6. The connecting point between the stable and unstable branches moves to a larger photon energy compared to the case in Fig. 6, indicating a larger upward shift of the threshold. The imaginary part has a broader profile in Fig. 7. We will investigate B_r -dependence more systematically for the refractive index in Sec. VB and the dielectric constant in Appendix A.

V. REFRACTIVE INDEX IN THE LLL APPROXIMATION

Thus far, we have considered only the dielectric constants ϵ . However, in some cases, it is more convenient to treat the refractive indices n , which can be immediately obtained from the dielectric constants through a simple relation $n^2 = \epsilon$. In this section, we will present results for the refractive index in the LLL approximation, and in particular we will focus on its dependences on the angle and magnetic field strength.

When the dielectric constants have imaginary parts, $\epsilon = \epsilon_{\text{real}} + i\epsilon_{\text{imag}}$, we can similarly define real and imaginary parts of the refractive indices as $n = n_{\text{real}} + in_{\text{imag}}$, which are explicitly given with respect to the refractive index as,

$$n_{\text{real}} = \frac{1}{\sqrt{2}}\sqrt{|\epsilon| + \epsilon_{\text{real}}}, \quad (19)$$

$$n_{\text{imag}} = \frac{1}{\sqrt{2}}\sqrt{|\epsilon| - \epsilon_{\text{real}}}, \quad (20)$$

with the magnitude $|\epsilon|$ being defined by $|\epsilon| = \sqrt{\epsilon_{\text{real}}^2 + \epsilon_{\text{imag}}^2}$.

As we saw in the previous sections, only the parallel mode of the dielectric constant ϵ_{\parallel} remains nontrivial in the LLL approximation, and the same is true for the refraction index: we have only n_{\parallel} as a nontrivial mode. Figure 8 shows the refractive index n_{\parallel} at $B_r = 500$ as a function of (scaled) photon energy squared $\tilde{\omega}^2$ that corresponds to the dielectric constant in Fig. 6. We find that the refractive index has a similar structure in photon energy dependence, and that it becomes complex when the dielectric constant takes the unstable branch. We do not repeat the explanation for the transition of the solutions from the naive prescription (I) to the fully self-consistent treatment (III). All the explanations for the dielectric constant ϵ_{\parallel} equally apply to the refractive index n_{\parallel} . In this section, we rather discuss dependences of the self-consistent solutions on the propagation angle θ and the magnetic field strength B_r . In fact, the same analyses were in advance performed for the dielectric constant ϵ_{\parallel} as summarized in Appendix A, and we have used those results to compute the refractive index through the relations (19) and (20).

A. Dependence on propagation angle

In the previous section and in Fig. 8, the results of ϵ_{\parallel} and n_{\parallel} were shown only for the angle $\theta = \pi/4$. However, there is a significant angle-dependence in the results, which we are going

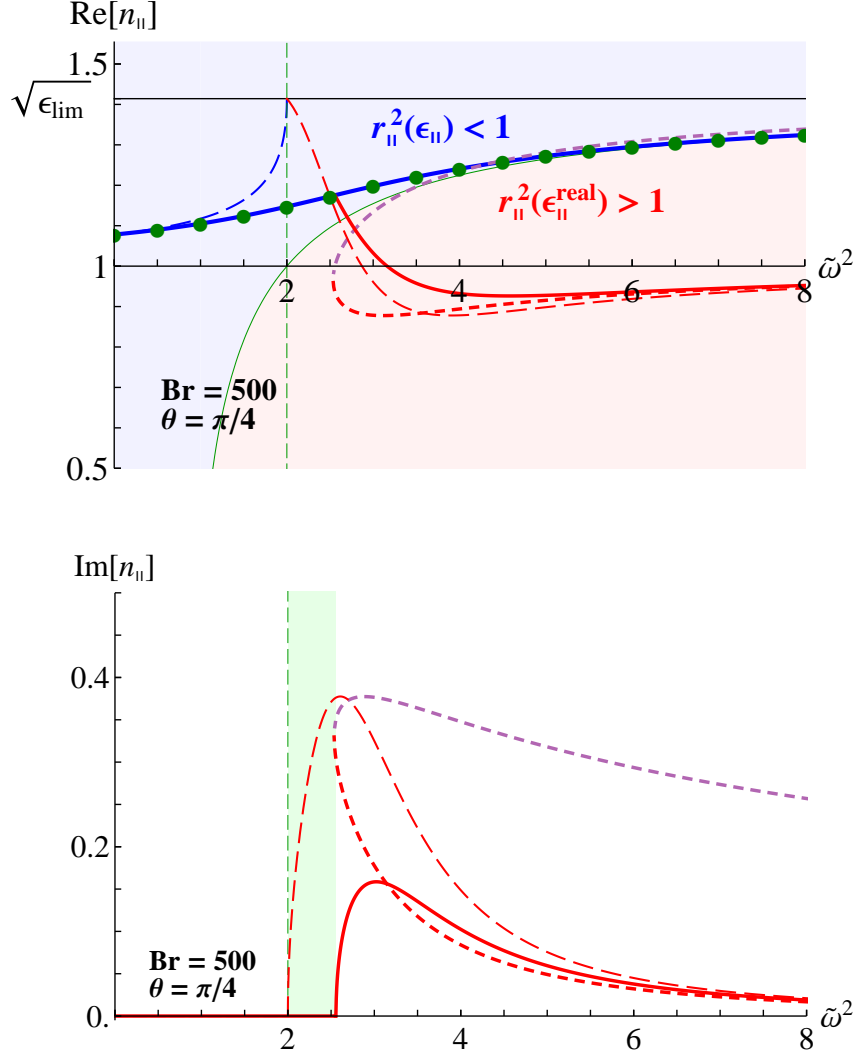


FIG. 8. Refractive index n_{\parallel} for $\theta = \pi/4$ and $B_r = 500$: each line shows the corresponding quantities explained in the legend in Fig. 6.

to present in this subsection. Upper and lower panels in Fig. 9 represent real and imaginary parts of the complex refractive index when the propagation angle varies from $\theta = 0$ to $\pi/2$. We have shown the results only in this region of θ because the refractive index has the following symmetry: $\epsilon_{\parallel}(\theta) = \epsilon_{\parallel}(-\theta) = \epsilon_{\parallel}(\pi \pm \theta)$. In the upper panel, solid lines are stable branches with different photon energies. A long-dashed line indicates a limiting value n_{lim} of the refractive index on the stable branch. It is given by $n_{\text{lim}} = \sqrt{\epsilon_{\text{lim}}} = |\cos \theta|^{-1}$, namely a square root of the limiting value of the dielectric constant (15). As seen in Fig. 8 for $\theta = \pi/4$, the refractive index approaches the limiting value n_{lim} as the photon energy increases. At a certain photon energy above around $\tilde{\omega}^2 \sim 1$, the refractive index on the stable branch strongly depends on the angle. The real parts grow with increasing θ , indicating that, when

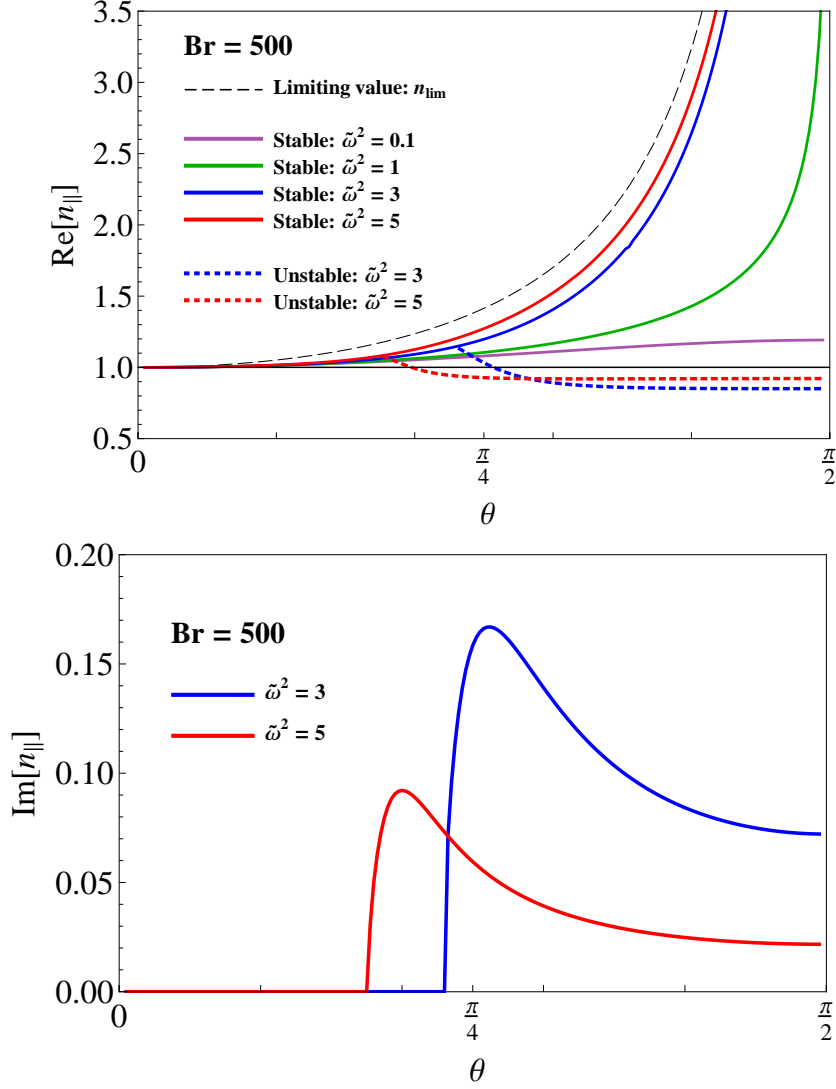


FIG. 9. Refractive index with varying propagation angle θ : The refractive index takes the same value, when photon propagation is oriented in the directions, $\pm\theta$, $\pi \pm \theta$.

a photon propagates almost perpendicularly to the magnetic field, the effects of vacuum birefringence appear more strongly and photon's phase velocity becomes significantly small.

While we obtained the simple expression of the limiting value n_{lim} within 1-loop accuracy of the vacuum polarization tensor, it is still an open question how higher-order diagrams contribute to the refractive index. Indeed, we notice that the limiting value n_{lim} diverges in particular two cases when the photon propagates in the perpendicular directions $\theta = \pm\pi/2$ with energy $\tilde{\omega}^2 = 1$. These singular behaviors would suggest that further careful investigation is required when the modification of the refractive index is very large, e.g., the

vacuum polarization would be suppressed by mutual Coulomb interaction between a fermion and antifermion pair appearing in the loop part which corresponds to photon exchanges in the multi-loop diagram.

There are also unstable branches (short-dashed lines) when the angle is large. This is clearly seen in the lower panel where the imaginary parts are shown. The stable (unstable) branches appear in small (large) θ region because the threshold condition $r_{\parallel}^2 = 1$ depends on the angle. Also, the angle where unstable branch starts to appear depends on the photon energy, and decreases with increasing energies. Therefore, if the photon energy is large enough, it can decay even at small angles. Note, however, that the decay never occurs at $\theta = 0$ within constant magnetic field case, where the refractive index persists to be unity as in the ordinary vacuum.

B. Dependence on the magnetic-field strength

In this subsection, we present the dependence of the refractive index on the magnitude of the external magnetic field. The real part of the refractive index on stable and unstable branches, and the imaginary part on the unstable branch are respectively shown below.

1. Real part

Upper panel of Fig. 10 shows a B_r -dependence of the refractive index n_{\parallel} on the stable branch. Since the stable branch is in the region below the threshold, the refractive index has only a real part. Curves and dots indicate the results from the LLL approximation and the numerical integration, respectively, which agree well with each other in the strong-field limit $B_r \gtrsim 10$. Thus, we again confirm the validity of the LLL approximation when the magnetic field is strong enough $B_r \gtrsim 10$. We find that, at any photon energy, magnitude of the refractive index increases with increasing B_r , and saturates in the limit of strong magnetic field. The limiting value is given by $n_{\text{lim}} = \sqrt{\epsilon_{\text{lim}}}$ as mentioned in the last subsection. While we discussed this limiting value n_{lim} as reached in the limit of a large photon energy (see Eq. (18)), the plot shows the same limit is reached, at any photon energy, in the strong-field limit. Remind that the limiting value of the dielectric constant ϵ_{lim} is obtained in the limit in which the scalar function χ_1 becomes divergently large $\chi_1 \gg 1$ as the photon momentum

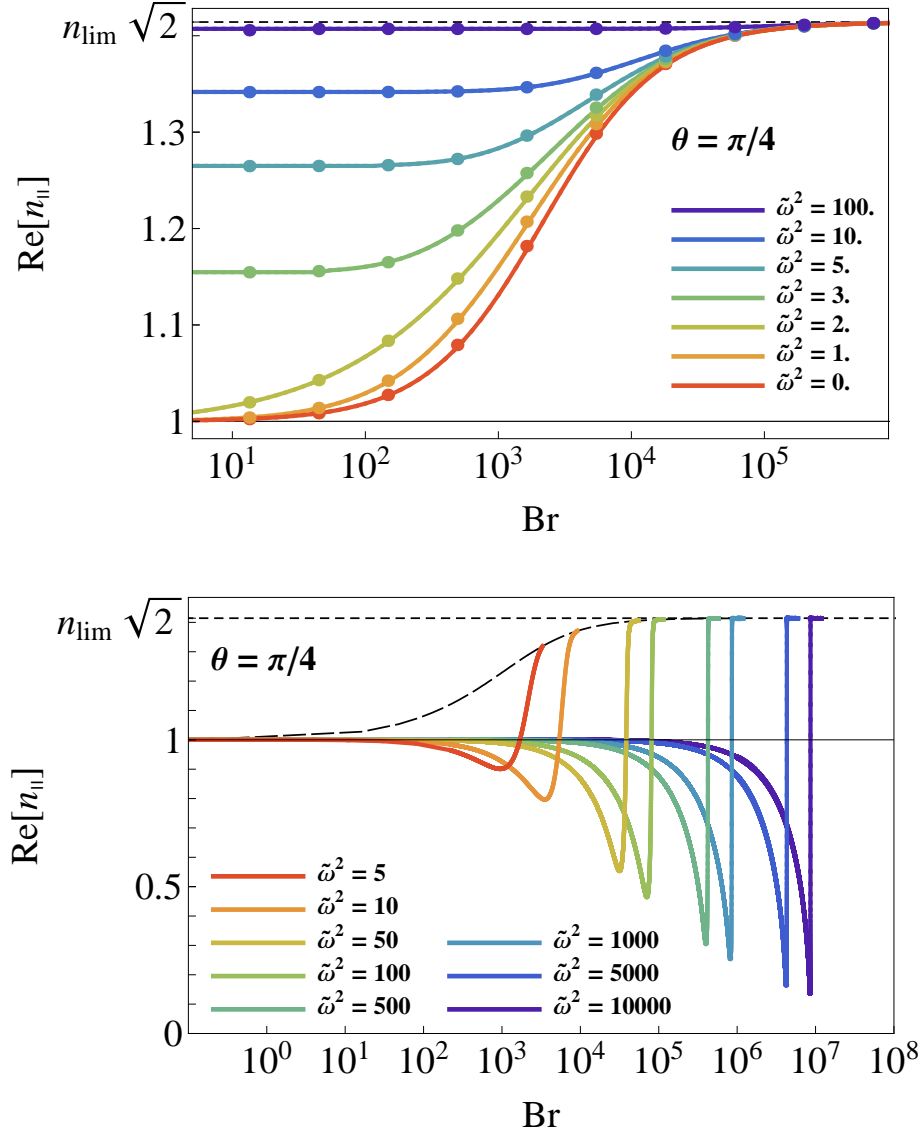


FIG. 10. B_r dependence of the real part of n_{\parallel} in the LLL approximation. Lines show the refractive index at $\theta = \pi/4$ and various photon energies. Upper and lower panels show the stable and unstable branches, respectively. In the upper panel, results from the LLL approximation agree well with those from the numerical integration which are indicated with dots.

approaches the threshold $r_{\parallel}^2(\epsilon_{\parallel}) \rightarrow 1$. Note also that the scalar function (9) is proportional to the field strength, $\chi_1 \propto B_r$, showing a divergently large value also in the strong field limit (see also Fig. 4). Therefore, even at a small photon energy, the dielectric constant approaches the limiting value ϵ_{lim} when the magnetic field is strong enough.

In the limit of zero frequency $\tilde{\omega}^2 = 0$, both r_{\perp}^2 and r_{\parallel}^2 are vanishing, and the scalar coefficient function χ_1^{LLL} has a simple form (see Eq. (9)),

$$\chi_1^{\text{LLL}}(0) = \frac{\alpha}{3\pi} B_r \quad , \quad (21)$$

which indicates a monotonic increase with respect to B_r . Thus, χ_1^{LLL} becomes of the order $\chi_1^{\text{LLL}} \sim 1$ if the magnetic field is as strong as $B_r \sim 3\pi/\alpha \sim 10^3$. Beyond this field strength, χ_1 starts dominating unities in the denominator and numerator in Eq. (12). Then, the dielectric constant and thus the refractive index would start approaching the limiting values ϵ_{lim} and n_{lim} , respectively. The upper panel in Fig. 10 shows sizable modification of the refractive index already around $B_r \sim 10^3$ at zero and low energies ($B_r = 3\pi/\alpha$ gives $n_{\parallel} = 4/3$ when $\theta = \pi/4$).

As the photon energy becomes large beyond $\tilde{\omega}^2 = 1/(1 - \cos^2 \theta)$ ($\tilde{\omega}^2 = 2$ when $\theta = \pi/4$ in Fig. 10), the refractive index is subject to significant modification even in a relatively weak regime, $B_r \lesssim 100$. This is because the squared momentum approaches the threshold $r_{\parallel}^2(\epsilon_{\parallel}) = 1$, and thus χ_1 increases divergently (see Fig. 3).

Lower panel in Fig. 10 shows the real part of the refractive index on the unstable branch. In this plot, each line has an end point at a certain B_r , because the unstable branch does not exist below a connection point between the stable and unstable branches, as shown in Fig. 8. Black long-dashed curve shows location of the connection point specified by a pair of photon energy and magnetic field strength. As found in a comparison between Fig. 6 and Fig. 7, the connection point shifts to a larger photon energy as B_r increases. Therefore, for a given photon energy, unstable branch does not exist above a certain magnetic field strength. Although peaks apparently look sharper as the photon energy increases, this is due to a logarithmic scale for the horizontal axis.

2. Imaginary part

Figure 11 shows B_r -dependence of the imaginary part of the refractive index on the unstable branch. As in the case of the real part shown in the lower panel in Fig. 10, there is a peak structure just below the end point of each curve, reflecting a prominent photon decay rate near the connection point. As we found in the comparison between Fig. 6 and Fig. 7, the threshold obtained in the self-consistent solution (the connection point) shifts more distantly

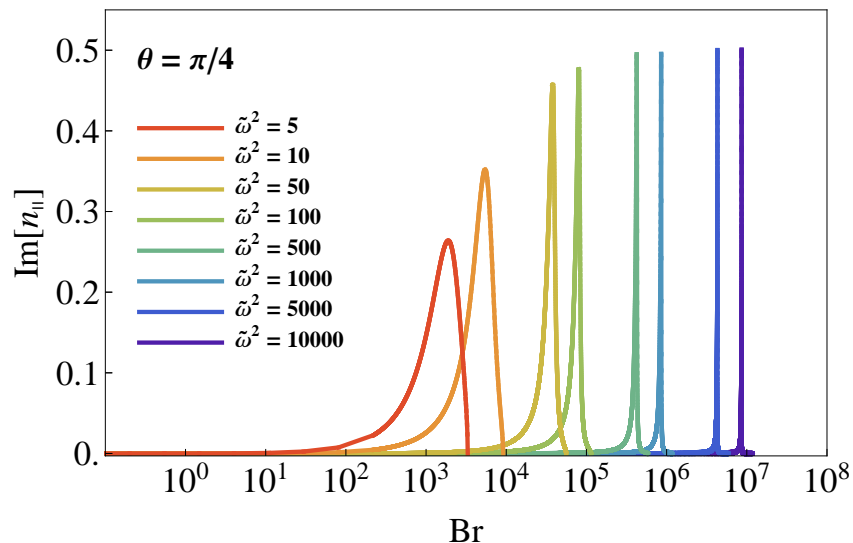


FIG. 11. B_r dependence of the imaginary part of $n_{||}$ on the unstable branch. Curves show those at $\theta = \pi/4$ and various photon energies.

from the naive one $\tilde{\omega}_{\text{th}}^2 = 1/\sin^2 \theta$ to a large photon energy when the magnetic-field strength is larger. Consistently to what we found there, a stronger magnetic field gives rise to the peak for an energetic photon in Fig. 10.

3. Real vs imaginary part on the unstable branch

Figure 12 shows a relation between real and imaginary parts of the complex refractive index on the unstable branch. The magnitude of the external magnetic field is fixed on each arc, and a radius increases as the magnetic field strength becomes larger. A gradation of colors transits from red to violet as the photon energy increases, of which scale is fixed so that the full range from red to violet appears on the innermost arc. Every arc has a left edge located on $\epsilon_{||} = 1 + 0 \cdot i$, because the refractive index on the unstable branch converges to unity in case of the strong-field limit within the LLL approximation, when the photon energy becomes large beyond the first threshold and stays small enough not to approach the second threshold. The opposite edge corresponds to the connection point between the stable and unstable branches. The imaginary part of the refractive index vanishes at this point, and the real part becomes large as the field strength becomes large. Magnitudes of the modification of the real and imaginary parts are comparable to each other at a fixed B_r .

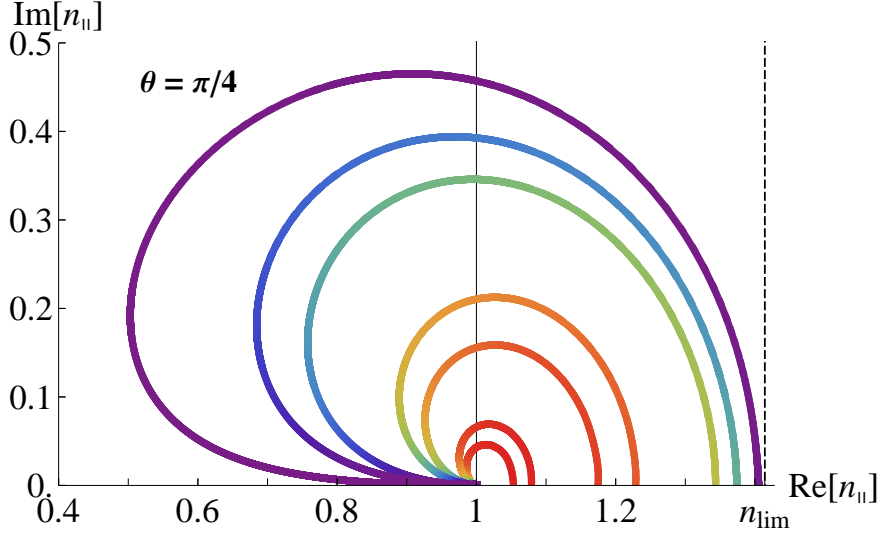


FIG. 12. Trajectories in a complex n_{\parallel} -plane showing its magnitudes on the unstable branch: The propagation angles are commonly fixed at $\theta = \pi/4$, and the magnetic field strength on each trajectory is taken as $B_r = \{50, 100, 500, 1000, 5000, 10000, 50000\}$ from the innermost to the outermost. On each curve, the photon energy increases from the right to left edges, where the right edge corresponds to the connection point between the stable and unstable branches.

C. Decay length

Lastly, let us show the decay length defined in Eq. (4). Figure 13 shows the decay length at a magnetic field strength $B_r = 500$ and propagation angles, $\theta = \pi/6, \pi/3, \pi/2$. Photon energy at the decay threshold becomes small as the angle increases, because of an angle dependence of the threshold condition, $r_{\parallel}^2 = 1$. While “magnetar” is thought to be accompanied by a strong magnetic field⁷ of order $B_r \sim 100$ extending in a macroscopic scale, plotted lines show that photon decays within order of 0.1 – 10 picometer if photon energy is above the threshold. This indicates a drastic modification of gamma-ray and dilepton spectra emitted from magnetars.

VI. SUMMARY AND DISCUSSIONS

We investigated the vacuum birefringence phenomena in strong magnetic fields on the basis of the analytic representation of the vacuum polarization tensor obtained in paper I

⁷ Here, physical scale is provided by the critical magnetic field strength defined by electron mass.

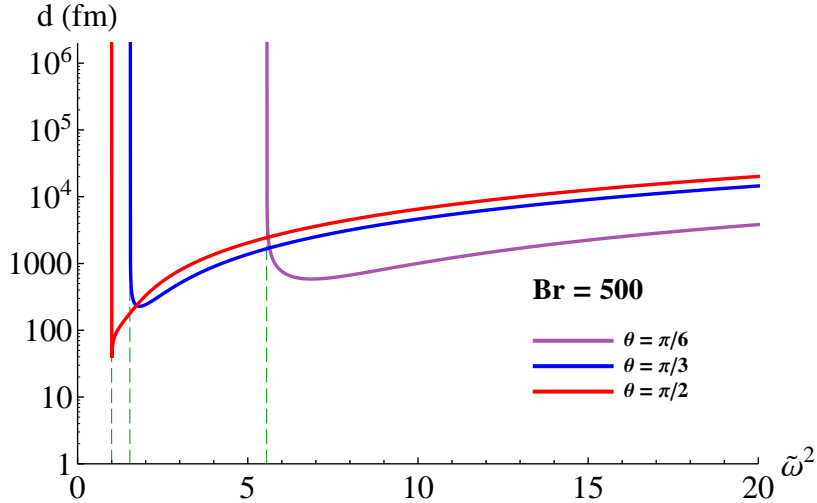


FIG. 13. Decay length of photon propagation in strong magnetic field: Photon decays within order of 0.1 – 10 picometer above the threshold, while magnetar has magnetic field extending in a macroscopic scale.

[1]. In particular, we analyzed in detail the phenomena in the lowest Landau level (LLL) approximation where both the dielectric constant (ϵ_{\parallel}) and the refractive index (n_{\parallel}) of a propagating photon in the mode parallel to the external magnetic field deviate from unity and become complex. The LLL contribution corresponds to the first term of the polarization tensor which is represented as the infinite sum with respect to the Landau levels, and turned out to be a very good approximation when the magnetic field is strong enough $B/B_c \gtrsim 1$ with B_c being the critical magnetic field strength for the relevant fermions.

In the LLL approximation, there is a threshold in the photon energy beyond which both ϵ_{\parallel} and n_{\parallel} acquire imaginary parts and thus the decay of a real photon into a pair of a fermion and an antifermion (in the LLLs) becomes possible. With the explicit analytic expression for the polarization tensor, we were able to thoroughly inspect properties of ϵ_{\parallel} and n_{\parallel} such as the dependences on the propagating angle and the magnetic-field strength, and also how the imaginary parts appear.

We found that the equations that define ϵ (or equivalently n) with respect to the scalar coefficient functions in the polarization tensor are implicit functions of ϵ (or n), and must be solved self-consistently in terms of ϵ (or n). This self-consistent procedure is indispensable for accurate description of ϵ and n when the deviation of ϵ and n from unity is large, which

is realized in the limit of strong fields or high-energy photons. Physically, this procedure is necessary for consistently taking into account the back reaction from the distorted Dirac sea in response to an incident photon field. Namely, an induced polarization and the photon decay bring in modifications of the external momentum, and thus dispersion, of the incident photon.

It is quite instructive to recognize that emergence of complex refractive indices can be seen even in a simple example, the dipole oscillator model, of an optical medium (see Refs. [13, 14] for pedagogical descriptions). The simplest case assumes that the medium is composed of many damped harmonic oscillators with a single resonant frequency ω_0 . The refractive index of this model has both real and imaginary parts, as shown in the left panel of Fig. 14. The imaginary part appears when the real part rapidly varies around the resonant frequency $\omega = \omega_0$, which corresponds to a negative slope in the dispersion (see the right panel of Fig. 14). This rapid change of the real part across unity and emergence of a peak of the imaginary part are qualitatively similar to the behaviors seen in Fig. 8. Consequently, a dispersion curve in Fig. 15, following the blue solid curve from the low photon energy up to the junction point and then the red curve, corresponds to the blue line in the right panel of Fig. 14. The dispersions in our result and the dipole oscillator model have a similar structure to each other, except two differences: that is, there is a definite threshold for the emergence of the imaginary part located on the lowest Landau level and the “stable” branch extends into infinite $\tilde{\omega}^2$ giving a double-valued refractive index above the threshold.

Now let us suppose that a photon enters into the dielectric medium from the ordinary vacuum, as an analogue of the case incident into strong magnetic fields. Dispersion relation of the photon will change from the linear relation (a dashed line in the right panel of Fig. 14) to that in the medium (a blue curve in Fig. 14). At the boundary, according to the Huygens-Fresnel principle, the direction of the light front will be modified consistently to the change of light velocity, while the frequency (photon energy) is conserved. Therefore, the incoming photon with $(\omega_{\text{vac}}, q_{\text{vac}})$ on the linear dispersion will move to $(\omega_{\text{med}} = \omega_{\text{vac}}, q_{\text{med}})$ on the curved dispersion line ($q_{\text{med}} \neq q_{\text{vac}}$). This argument does not prohibit transition to any in-medium dispersion as long as the energy conservation is satisfied, and, if the incident light is intense enough, a nonlinear response of the dielectric medium to the light generates higher harmonic waves, so that even transitions to other frequencies could become possible. Then, what happens in the case with the vacuum birefringence in strong magnetic fields?

Having performed self-consistent treatment, we found the refractive index as a double-valued function of the photon energy that is composed of stable and unstable branches shown in Fig. 8 or in Fig. 15. If one considers an incoming photon from the vacuum into the region with a strong magnetic field, one encounters a problem that there are two possible transitions (one is onto the red curve and the other, blue) when the photon energy is high enough. Assuming that the transitions to both the branches are possible, it would be natural that the transition to the closer branch is preferred. Thus, which branch is realized depends on the dispersion of the incoming photon outside the magnetic field as well as the detailed structure of the dispersion in the magnetic field. As far as the photon enters from the vacuum, we expect that the unstable branch would be more preferably realized in case shown in Fig. 15.

We also call attention to a similarity between dispersions in our result and of “polariton” which is a resonant state arising in a coupling between a quasi-particle and a photon. Dispersion relation of a polariton typically has two separate branches with a level repulsion at the crossing point of the original dispersions of those constituent particles. More specifically, there are some well-known polaritons, e.g., called “exciton polariton”, “surface plasmon polariton” and “phonon polariton”, excited when a photon couples to a particle-hole excitation in semiconductors, a quantized plasma oscillation in the vicinity of metal surfaces and a phonon in crystals, respectively (see Sec. 4, 7.5 and 10.3 in Ref. [14]). They have been indeed observed in experiments. However, polaritons can be excited only when the dispersion of a probe photon incident into the substances has an intersection with the polariton dispersion curves, while we argued on the basis of an analogy with the classical dipole oscillator that the transition to any branch is in principle possible within a certain probability. Nevertheless, both of these analogies indicate that the dispersion outside the medium also plays an important role as an initial condition for realization of the in-medium propagating modes.

Although these analogies seem not to be totally suitable to the present case, they could provide clues to grasp intuitive understandings and prospects. A “selection rule” for the transitions onto the branches will be studied elsewhere.

Lastly, let us compare our results with the refractive indices which we encounter in ordinary life, and discuss possible applications to the physical situations accompanied with strong magnetic fields. The refractive index acquires a large value in the strong field limit. For example, at the angle $\theta = \pi/4$, the refractive index n_{\parallel} keeps increasing with stronger

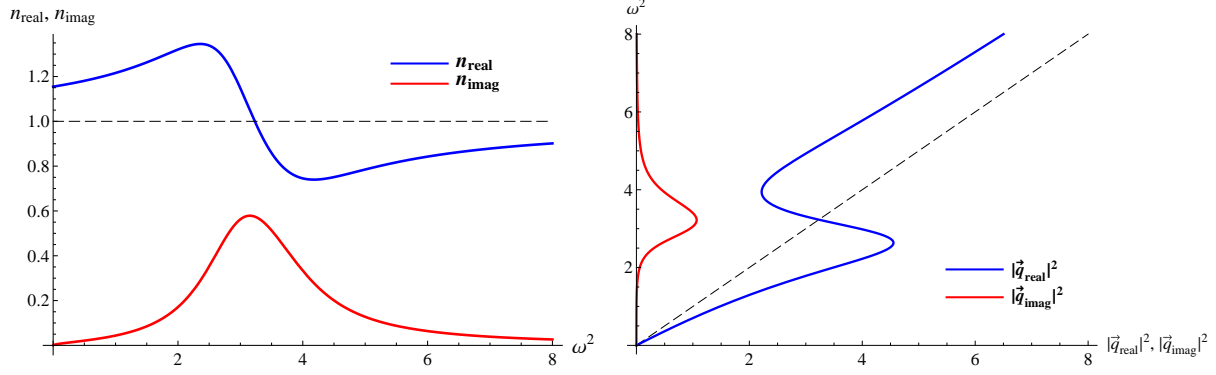


FIG. 14. (Left) Refractive indices of a simple damped harmonic oscillator model. (Right) Dispersion of a propagating photon in a dielectric medium. Blue and red lines are, respectively, the real and imaginary parts of the refractive index. Dashed lines are the refractive index $n = 1$ (left) and the dispersion $\omega = |\vec{q}_{\text{real}}|$ of a photon in a vacuum (right). Energy and momentum are taken in arbitrary unit for an illustration.

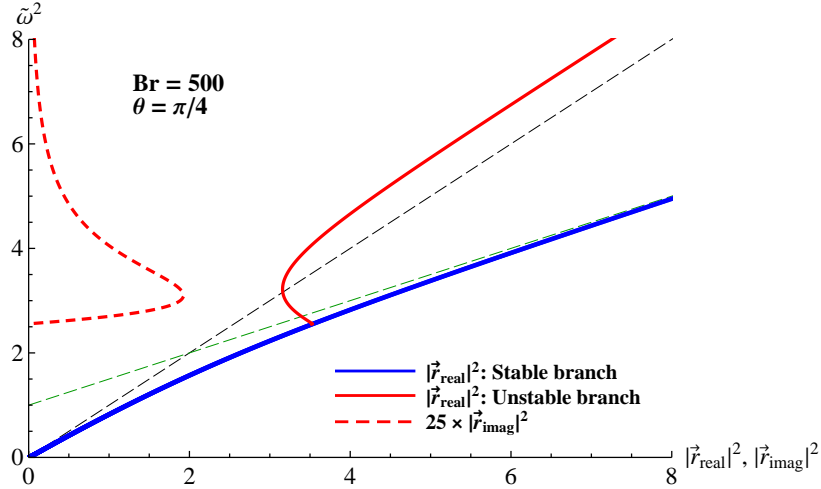


FIG. 15. Dispersion relation of a photon propagating in a strong magnetic field. The propagation angle and the magnetic field strength, shown in the legend, are taken as in Fig. 8.

magnetic fields, and approaches the limiting value $n_{\text{lim}} = \sqrt{2}$. This is comparable to the values which we encounter in ordinary life. To name a few, atmosphere of the earth (1 atm, 0 °C) and water (20 °C) have refractive indices, $n_{\text{air}} = 1.000293$ and $n_{\text{water}} = 1.333$, respectively, and “calcite” known as a representative birefringent material has refractive indices $n_o = 1.6584$ and $n_e = 1.4864$ for ordinary and extraordinary modes, respectively. At a mag-

netic field strength $B_r \sim (m_\pi/m_e)^2 \sim 10^{4-5}$ which could be realized in the ultrarelativistic heavy-ion collisions⁸ [15–18], the refractive index is close to the limiting value $n_{\text{lim}} = \sqrt{2}$, and thus can be larger than that of gas, and even comparable to those of liquid and solid.

An accurate description of the complex refractive index across the lowest threshold will be directly applicable to the studies of intriguing phenomena in magnetars whose magnetic field is estimated to be two orders larger than the critical magnetic field strength [19, 20]. In particular, descriptions of both the real and imaginary parts will work as robust building blocks necessary for investigating the interplay and competition among photon splitting, vacuum birefringence and photon decay [21, 22].

Besides, as mentioned above, the ever strongest magnetic field will be created in the ultrarelativistic heavy-ion collisions in RHIC and LHC experiments. Since the magnitude of the magnetic field could be four orders larger than the critical magnetic field, radiations from the created matter in collision events would interact with the extremely strong magnetic fields, and bring out the information of the early-time dynamics [23, 24]. However, photons created in heavy-ion collisions have, in general, large energies. Thus we need to extend the present work towards including important contributions among all the Landau levels shown in paper I.

In application to laser physics [25], it will be very important to include effects of a strong electric field as well as a magnetic field. For this sake, basic concepts and techniques examined in this series of papers could be useful to find differences out of similarities between expressions of the vacuum polarization tensors in the presence of external electric and magnetic fields.

ACKNOWLEDGEMENTS

The research of KH is supported by the Korean Ministry of Education through the BK21 Program. This work was also partially supported by Korea national research foundation under grant number KRF-2011-0030621 and “The Center for the Promotion of Integrated Sciences (CPIS)” of Sokendai.

⁸ m_π and m_e are masses of a pion $m_\pi \sim 140$ MeV and an electron $m_e \sim 0.5$ MeV, respectively.

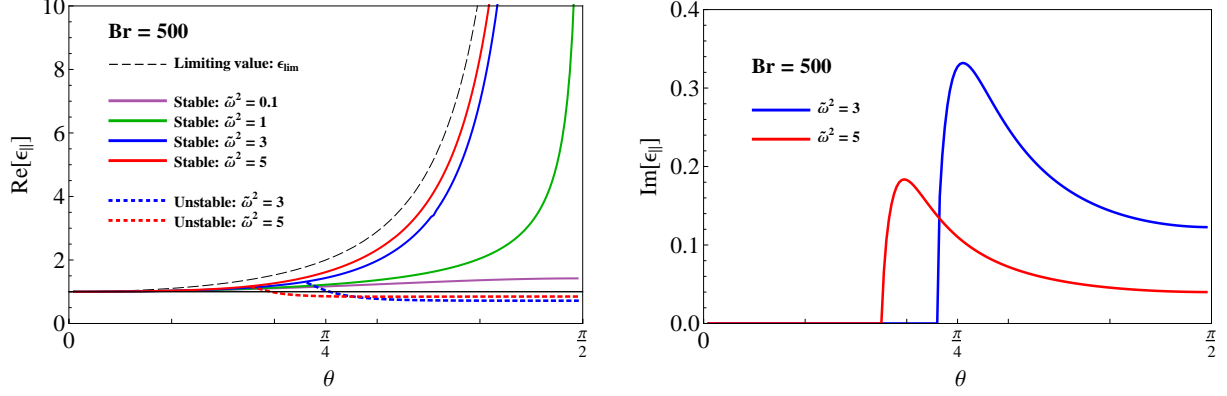


FIG. 16. Dependence of ϵ_{\parallel} on photon's propagation angle θ : Parameters are the same as in Fig. 9. Dashed line shows the limiting value (15).

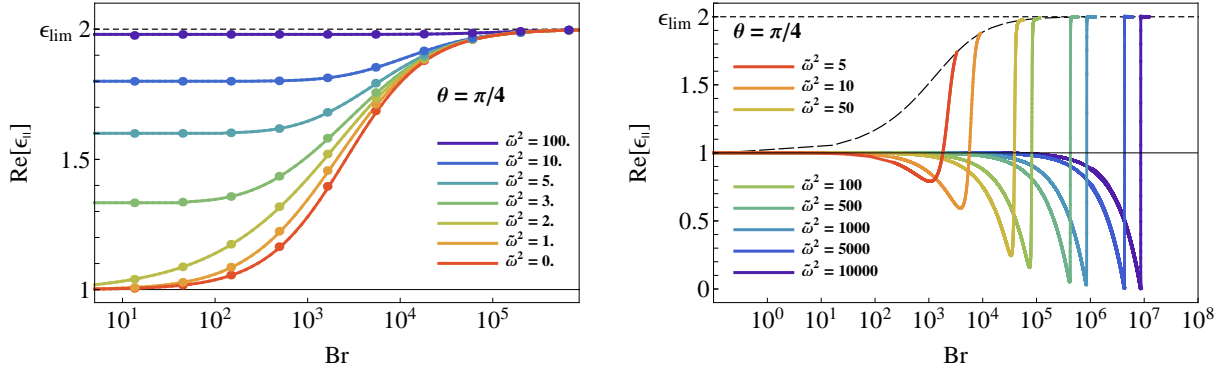


FIG. 17. B_r dependence of the real part of ϵ_{\parallel} on the stable (left) and unstable (right) branches. Photon's propagation angle is fixed at $\theta = \pi/4$, and photon energies are varied as indicated in the panels. Dielectric constant on the stable branch, obtained from the numerical integration, is shown with dots in the left panel.

Appendix A: Dependence of the dielectric constant on B_r and θ

In this supplementary section, we show dependences of the dielectric constant ϵ_{\parallel} on the propagation angle θ and the magnetic-field strength B_r . By self-consistently solving Eq. (12), we obtained plots shown in Figs. 16 – 19, which are then mapped to the refractive index through the relations (19) and (20) to yield Figs. 9 – 12. Parameters in these plots are taken as the same values as those in the corresponding plots of the refractive index in Fig. 9 – 12. The dependence on the photon's propagation angle is shown in Fig. 16. The real part of the dielectric constant on the stable and unstable branches are shown in the left and right panels in Fig. 17, respectively, while the imaginary part on the unstable branch is shown

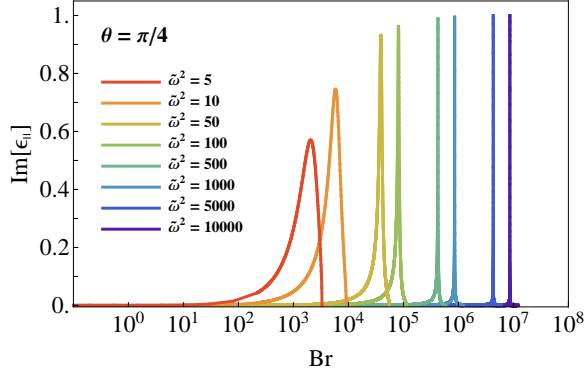


FIG. 18. B_r -dependence of the imaginary part of ϵ_{\parallel} on the unstable branch. Parameters are the same as in the right panel of Fig. 17.

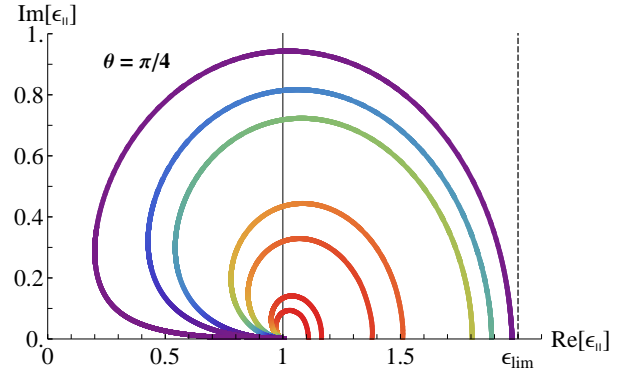


FIG. 19. Trajectories on a complex ϵ_{\parallel} -plane. Parameters are the same as in Fig. 12.

in Fig. 18. Magnitudes of the real and imaginary parts on the unstable branch are shown together in Fig. 19 as contours in the complex ϵ_{\parallel} -plane.

Appendix B: Remark on other Landau levels

We remark on structures near the thresholds in other Landau levels which have the same property as that of the lowest Landau level. In the infinite series expression of the scalar coefficient functions χ_i with all the Landau levels (see Sec. IV in paper I [1]), we find a relation between the coefficient functions $\chi_0 = -\chi_2$, if we pick up an individual contribution specified by $\ell = 0$ and $n (\neq 0)$. It immediately follows from Eq. (1) that the dielectric constant of the perpendicular mode is then given by

$$\epsilon_{\perp} = \frac{1 + \chi_0}{1 + \chi_0 \cos^2 \theta} . \quad (\text{B1})$$

The right-hand side of the above expression has the same form as Eq. (12), except that the scalar function χ_1 is replaced by χ_0 . Because χ_0 diverges at these thresholds as χ_1 does at the lowest threshold, the dielectric constant has a limiting value,

$$\lim_{r_{\parallel}^2 \rightarrow s_+^{0n}} \epsilon_{\perp}(r_{\parallel}^2) = \frac{1}{\cos^2 \theta} , \quad (\text{B2})$$

when the photon momentum approaches the thresholds as $r_{\parallel}^2 \rightarrow (1 + \sqrt{1 + 2nB_r})^2/4 \equiv s_+^{0n}$. The right-hand side of Eq. (B2) is exactly the same as that of Eq. (15). Therefore, the

dielectric constant ϵ_{\perp} in the perpendicular mode would, in the region around the thresholds at $\ell = 0$ and $n(\neq 0)$, have the same structure in the photon energy dependence as that of the longitudinal mode ϵ_{\parallel} around the lowest threshold.

-
- [1] K. Hattori and K. Itakura, “*Vacuum birefringence in strong magnetic fields: (I) Photon polarization tensor with all the Landau levels*”, Ann. Phys. **330** (2013) 23-54. [arXiv: 1209.2663 \[hep-ph\]](https://arxiv.org/abs/1209.2663) .
- [2] D. Melrose and R. Stoneham, Nuovo Cimento A **32** (1976) 435.
- [3] W. Tsai, Phys. Rev. D **10** (1974) 2699.
- [4] L. F. Urrutia, Phys. Rev. D **17** (1978) 1977.
- [5] S. L. Adler, Ann. Phys. **67** (1971) 599-647.
- [6] W. Tsai and T. Erber, Phys. Rev. D **10** (1974) 492; *ibid.*, Phys. Rev. D **12** (1975) 1132.
- [7] W. Dittrich and M. Reuter, Lect. Notes Phys. **220** (1985) 1-244.
- [8] W. Dittrich and H. Gies, Springer Tracts Mod. Phys. **166** (2000) 1-241.
- [9] J. S. Schwinger, Phys. Rev. **82** (1951) 664-679.
- [10] K. Fukushima, Phys. Rev. D **83** (2011) 111501.
- [11] V. P. Gusynin, V. A. Miransky and I. A. Shovkovy, Nucl. Phys. B **462** (1996) 249-290.
- [12] K. Kohri and S. Yamada, Phys. Rev. D **65** (2002) 043006.
- [13] E. Hecht, “*Optics, fourth edition*”, Addison-Wesley (2001).
- [14] M. Fox, “*Optical properties of solids, second edition*”, Oxford University Press (2010).
- [15] D. E. Kharzeev, L. D. McLerran, and H. J. Warringa, Nucl. Phys. A **803** (2008) 227-253.
- [16] V. Skokov, A. Y. Illarionov and V. Toneev, Int. J. Mod. Phys. A **24** (2009) 5925-5932; A. Bzdak and V. Skokov, Phys. Lett. B **710** (2012) 171-174.
- [17] W. T. Deng and X. G. Huang, Phys. Rev. C **85** (2012) 044907.
- [18] K. Itakura, “*Strong Field Physics in High-Energy Heavy-Ion Collisions*”, in “*Proceedings of International Conference on Physics in Intense Fields (PIF2010)*,” (K. Itakura, et al. (eds.)) 24-26 November 2010, KEK, Tsukuba, Japan, available from <http://ccdb5fs.kek.jp/tiff/2010/1025/1025013.pdf>
- [19] C. Thompson and R. C. Duncan, Mon. Not. Roy. Astron. Soc. **275** (1995) 255; *ibid.*, Astrophys. J. **473** (1996) 322.

- [20] A. K. Harding and D. Lai, Rept. Prog. Phys. **69** (2006) 2631. [arXiv: 0606.674 \[astro-ph\]](#).
- [21] S. L. Adler, et al., Phys. Rev. Lett. **25** (1970) 1061-1065.
- [22] M. G. Baring, “*Photon Splitting and Pair Conversion in Strong Magnetic Fields,*” AIP Conf. Proc. **1051** (2008) 53. [arXiv: 0804.0832 \[astro-ph\]](#).
- [23] K. Tuchin, Phys. Rev. C **82** (2010) 034904; *ibid.*, Phys. Rev. C **83** (2011) 017901; *ibid.*, “*Electromagnetic radiation by quark-gluon plasma in magnetic field*”, [arXiv: 1206.0485 \[hep-ph\]](#).
- [24] K. Itakura and K. Hattori, “*Effects of extremely strong magnetic field on photon HBT interferometry*”, PoS *WPCF2011* (2011) 042. [arXiv: 1206.3022 \[nucl-th\]](#).
- [25] Euro. Phys. J. D, Volume 55, Number 2 / November 2009 “*Topical issue on Fundamental physics and ultra-high laser fields*”.